

---

# LATENT REPRESENTATION LEARNING OF MULTI-SCALE THERMOPHYSICS: APPLICATION TO DYNAMICS IN SHOCKED POROUS ENERGETIC MATERIAL

---

Shahab Azarfar<sup>1</sup>, Joseph B. Choi<sup>1</sup>, Phong CH. Nguyen<sup>1</sup>, Yen T. Nguyen<sup>2</sup>, Pradeep Seshadri<sup>2</sup>, H.S. Udaykumar<sup>2</sup>, and Stephen Baek<sup>1,3,\*</sup>

<sup>1</sup>School of Data Science, University of Virginia, United States

<sup>2</sup>Department of Mechanical Engineering, University of Iowa, United States

<sup>3</sup>Department of Mechanical and Aerospace Engineering, University of Virginia, United States

\*Corresponding Author: baek@virginia.edu

June 17, 2025

## ABSTRACT

Coupling of physics across length and time scales plays an important role in the response of microstructured materials to external loads. In a multi-scale framework, unresolved (subgrid) meso-scale dynamics is upscaled to the homogenized (macro-scale) representation of the heterogeneous material through closure models. Deep learning models trained using meso-scale simulation data are now a popular route to assimilate such closure laws. However, meso-scale simulations are computationally taxing, posing practical challenges in training deep learning-based surrogate models from scratch. In this work, we investigate an alternative meta-learning approach motivated by the idea of tokenization in natural language processing. We show that one can learn a reduced representation of the micro-scale physics to accelerate the meso-scale learning process by tokenizing the meso-scale evolution of the physical fields involved in an archetypal, albeit complex, reactive dynamics problem, *viz.*, shock-induced energy localization in a porous energetic material. A probabilistic latent representation of *micro*-scale dynamics is learned as building blocks for *meso*-scale dynamics. The *meso*-scale latent dynamics model learns the correlation between neighboring building blocks by training over a small dataset of meso-scale simulations. We compare the performance of our model with a physics-aware recurrent convolutional neural network (PARC) trained only on the full meso-scale dataset. We demonstrate that our model can outperform PARC with scarce meso-scale data. The proposed approach accelerates the development of closure models by leveraging inexpensive micro-scale simulations and fast training over a small meso-scale dataset, and can be applied to a range of multi-scale modeling problems.

**Keywords** Meta-learning · scientific machine learning · surrogate modeling · multi-scale dynamics

## 1 Introduction

Multi-scale dynamics, coupling phenomena at two or more distinct scales, arise in many physical applications, such as multi-phase flows [1, 2], transport in porous media [3, 4], multi-material flows [5, 6], etc. When scales are distinctly separated, distinguished by the presence of an underlying microstructure, for example [7], the conventional practice is to solve the dynamics at the observable (macro-) scale by homogenizing the properties and processes of the unresolved (micro-/meso-) scale. This leads to the need for closure models to connect physics across disparate scales.

Scale bridging has been accomplished in a variety of ways [8, 9, 10]; in recent times, data-driven closure models have been developed using highly resolved direct numerical simulations (DNS) to inform machine learning algorithms [11, 12, 13]. The machine learned models serve as surrogates to close macro-scale dynamics. With the exponential rise

of deep learning (DL) [14, 15], artificial intelligence (AI)/machine learning (ML) has received a great deal of research attention in the context of scale-bridging for multi-scale dynamics problems. In particular, physics-informed machine Learning (PIML) [16] approaches seek to assimilate sub-grid dynamics in deep neural networks (DNNs), and a wide range of capabilities for multi-scale modeling using these techniques are now available [17, 18, 19].

While these DNN-based approaches are powerful for data assimilation and representation, they are inherently data hungry, which places the onus on computationally intensive physical simulations to supply adequately rich datasets to the AI/ML model. In this paper, we propose a *meta-learning* framework in which one leverages an ensemble of inexpensive micro-scale simulations in order to accelerate the learning process of a surrogate model for the meso-scale dynamics.

Here, the meta-learning approach is applied to an archetypal multi-scale dynamics problem, namely the response of a porous energetic material (EM) to shock loading. EM (defining the broad class of propellants, explosives, and pyrotechnics) have complex microstructural morphologies, which strongly influence the performance characteristics of these materials [20]. Defects such as voids and cracks in the microstructure of EM are sites of energy localization, which can evolve into concentrated regions of high temperature called “hotspots” [21]. Under a strong shock condition, a major mechanism for the formation of hotspots is void collapse, which leads to energy release on a very short time-scale (*i.e.*, nanoseconds) [22, 23].

The problem of shock-induced energy localization in porous energetic material is inherently multi-scale in the following sense: at the micro-scale (*i.e.*,  $\mathcal{O}(1\ \mu\text{m})$ ), the collapse of isolated voids in the microstructure of an EM can create localized hotspots that may expand and lead to ignition of the surrounding material; the resulting hotspots can trigger chemical reactions that release further energy and intensify the traveling shockwave, which, eventually, can lead to a self-sustaining detonation at the macro-scale (*i.e.*,  $\mathcal{O}(1\ \text{mm})$ ).<sup>1</sup> For this to occur, however, the heat release from a large ensemble of hotspots must be coordinated with the overpassing shock, successively pumping energy into the shock all the way to the formation of a detonation wave, a phenomenon called shock-to-detonation transition (SDT) [24]. Thus, the presence of multitudes of potential localization sites in the stochastic microstructure of porous energetic materials needs to be simulated to model SDT [25].

Direct numerical simulations (DNS) play an important role in understanding the above-mentioned complex physics at the meso-scale [26, 27, 28, 29, 30]. Figure 1 (a) and (b) illustrate an instance of numerical simulation results representing the shock-induced temporal evolution of temperature and pressure fields associated with a micro-scale single-pore collapse [31] and a meso-scale field of voids in a domain of EM microstructure [29], respectively. The columns in the figures show a snapshot of the corresponding temperature and pressure fields at different instants of time (noted above the panels); In addition, there has been a recent interest in data-driven approaches, especially deep learning models, to learn surrogate models from simulation data, and make fast predictions of the corresponding dynamics with comparable accuracy to DNS [17]. However, the high computational cost of DNS for generating meso-scale numerical simulations poses practical challenges in data-driven approaches, which typically need relatively large datasets for training the models. Alleviating the need for computationally intensive meso-scale simulations motivates the current meta-learning strategy.

In general, the cross-disciplinary areas of meta-learning [32, 33] and transfer-learning [34, 35] consist of a class of machine learning methodologies that aim to learn a common “meta” information from a family of closely related tasks and use it to quickly adapt the learned model to new unseen tasks. We use an analogy between natural language processing (NLP) and the relation between micro- and meso-scale dynamics, associated with the response of microstructured material to external loads, in the following way: an important step in the learning process of an NLP model is the *tokenization* in which a piece of text, *e.g.*, a sentence or a paragraph, is broken down into meaningful chunks of information, *e.g.*, words, which are called *tokens* and can be considered as discrete building blocks of the original text. The tokenization lets an NLP model start by analyzing these building blocks, and in later steps, combine the token-level learned information to capture the correlation between tokens and learn higher-level information about the whole text.

Following the above-mentioned tokenization analogy, we consider the meso-scale dynamics (“paragraph”) as a *correlated* system of machine learning building blocks, where each constituent encodes a *reduced (latent) representation* of the micro-scale dynamics (“words”). The main hypothesis underlying our consideration of a reduced representation of micro-scale dynamics, as building blocks for meso-scale, is that the fine-grain and stochastic nature of the micro-scale physics has a negligible effect on the coarse-grain meso-scale behavior of the system, and it mostly gets smeared out from the statistical point of view. Therefore, we consider the direct sum of the reduced representations of the micro-scale dynamics, after applying the appropriate time-delay, as a “first order approximation” of the meso-scale

---

<sup>1</sup>In the context of porous energetic material, we refer to the length scale of a single pore (*i.e.*,  $\mathcal{O}(1\ \mu\text{m})$ ) and the length scale of a field of voids in a microstructure domain of size  $\mathcal{O}(100\ \mu\text{m})$  and  $\mathcal{O}(1\ \text{mm})$  as the micro, meso and macro-scale, respectively.

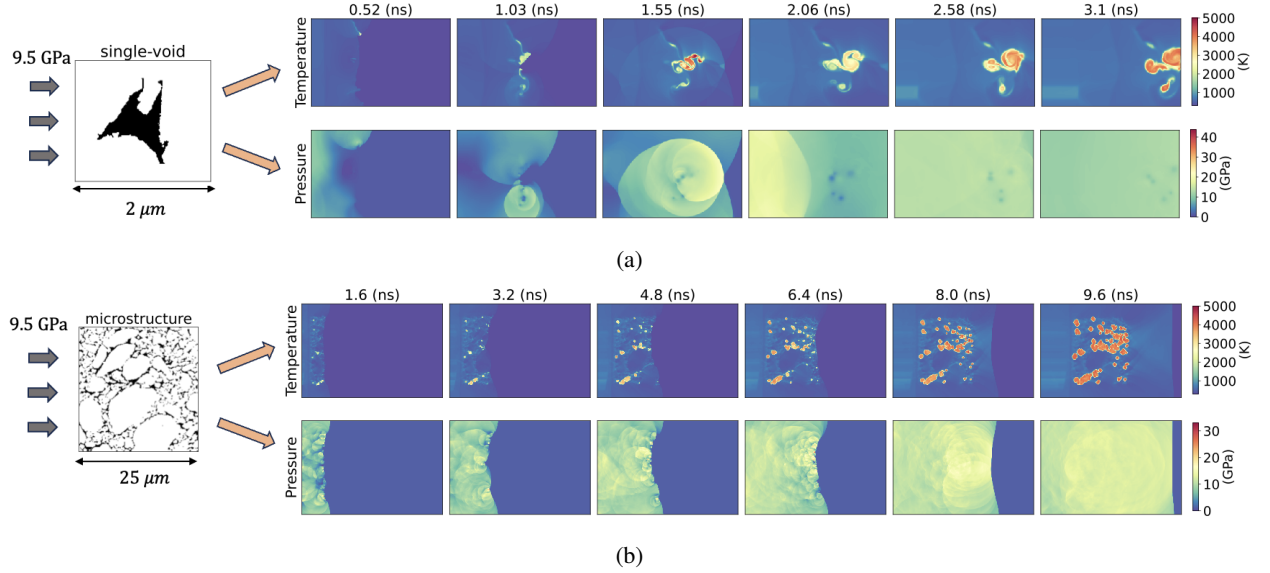


Figure 1: Temperature and pressure field evolution corresponding to (a) micro- and (b) meso-scale simulation of shock-induced energy localization in porous energetic material.

dynamics for a short time span. However, we assume that the interaction between these micro-scale building blocks would play a fundamental role in determining the meso-scale evolution of the corresponding physical fields. In other words, for longer time periods than the micro-scale temporal resolution, the evolution of physical fields over neighboring micro-scale building blocks will couple together, leading to deviation of the meso-scale dynamics from purely being the direct sum of micro-scale dynamics. The effects due to the correlation between neighboring micro-scale building blocks are considered as “higher order corrections.”

Therefore, the proposed meta-learning framework can be summarized, roughly, into two steps: in the first step, one learns a reduced representation of the micro-scale dynamics, as the building blocks of a “first order approximation” of the meso-scale dynamics, from a relatively large dataset of (inexpensive) micro-scale numerical simulations; in the second step, one learns the correlation between these building blocks, “higher order corrections,” from a relatively small dataset of (expensive) meso-scale simulations. In this paper, we test the hypothesis underlying the proposed meta-learning framework for the problem of shock-induced energy localization in porous energetic materials.

The structure of the paper is as follows. In Section 2, we provide an overview of the main ideas underlying our proposed approach, and explain how it can be connected to reduced order modeling and meta-learning. In Section 3, we present the detailed mathematical formulation and architecture of the model considered in this work. In Section 4, we present our proposed meta-learning framework applied to the problem of learning a surrogate model for the meso-scale dynamics associated with shock-induced energy localization in EM. Furthermore, we compare the prediction performance of our model with a physics-aware recurrent convolutional neural network (PARC), in the scarce meso-scale data regime, in terms of sensitivity quantities of interest (QoI) for EM. Also, the uncertainty in our model’s predicted QoI, due to the stochastic nature of learned dynamics over the latent space, is investigated. We conclude in Section 5 with a summary of our work and potential future directions for expanding the current work. Additionally, we provide details on implementation of our model and its training in Appendix A.1. In Appendix A.2, we discuss more details on the numerical simulation setup considered for generating the data used in this work.

## 2 Overview and Related Works

The proposed approach in this work combines ideas from reduced order modeling (ROM) [36] and meta-learning [32] in machine learning to accelerate the learning process of surrogate models for the meso-scale dynamics underlying the response of microstructured material to external loads, based on the relation between micro and meso-scale dynamics. In the following, we review the main ideas and the contribution of this work.

**Reduced Order Modeling** Almost all classical *projection-based* reduced order modeling methods, including Proper Orthogonal Decomposition (POD) [37] and Dynamic Mode Decomposition (DMD) [38], are based on considering a

projection onto a *linear subspace* of the full state space. However, the projection-based ROMs can only provide an accurate model in the case of problems with a fast-decaying Kolmogorov  $n$ -width, *e.g.*, diffusion-dominated problems, whose solution space can be well approximated by a linear subspace [39]. On the other hand, many physical problems of interest, including advection-dominated problems like shock-induced energy localization in EM, exhibit a slow-decaying Kolmogorov  $n$ -width, which necessitates the consideration of nonlinear techniques for approximating the solution space. Each of various nonlinear techniques in reduced order modeling try to approximate the *invariant (slow) manifold* [40, 41] of the corresponding dynamical system which can be defined as an attracting submanifold of the system’s full state space on which the dynamics is slow and free of high-frequency motions compared to the state space regions away from its basins of attraction (see, *e.g.*, [42, 43, 44]). In particular, the deep learning-based reduced order models (DL-ROMs) have become popular recently for learning nonlinear latent representations of physical dynamics in deep neural networks [45, 46, 47, 48, 49, 50]. However, to the best of our knowledge, most of DL-ROMs aim to learn a *deterministic* dynamics over the invariant manifold of the system which limits the generalizability and robustness of the model.

In contrast, we consider a *probabilistic* deep learning-based model which learns a *stochastic* dynamics over the latent space. This stochasticity play a crucial role in our model’s success in learning the meso-scale dynamics of shock-induced energy localization in EM in scarce data regimes. Our model consists of two main parts. In the first part, we use *variational autoencoders* (VAE) [51] to encode the corresponding system of coupled physical fields, whose evolution describes the dynamics in the full state space, into *discrete Gaussian random fields* as the associated latent representations. In the second part of our model, we learn the reduced dynamics of the corresponding Gaussian random fields using an *autoregressive* model. Motivated by the stochastic differential equation (SDE) formulation, the autoregressive functional of our model is decomposed into two parts: a *deterministic* part that captures the evolution of the latent mean fields over the slow manifold; and a *stochastic* part that encapsulates the evolution of the latent variance fields as the probabilistic deviation from the slow deterministic dynamics. We further decompose each of the deterministic and the stochastic autoregressive models into two functionals: a *decoupled* part which captures the short time-span evolution of each latent field corresponding to a single physical field, independent of the other physical fields; and a *correlation* part which encapsulates the interaction between all the involved physical fields in our multiphysics system. This strategy allows for learning the long-term global dynamics of coupled physical fields, which can involve distinct phases over different time periods, such as the hotspot ignition and growth phases in shock-induced energy localization in EM.

**Meta-Learning** Broadly speaking, meta-learning [52, 53] or *learning to learn* [54] refers to a bi-level learning process in which an *inner (base)* learning algorithm solves a particular task defined by a dataset and objective function, while an *outer (meta)* algorithm updates the inner learning algorithm such that the learned model improves an outer objective like generalization over a family of closely related tasks. The meta-learning approaches can be roughly divided into three main classes [55]: *i)* methods based on a bi-level optimization, where the inner algorithm learns the parameters of the model conditioned on certain hyperparameters and these hyperparameters are optimized in the outer level based on a meta-loss [56, 57, 58]; *ii)* methods that learn an outer-level metric space which is based on a notion of distance (similarity) between inner-level tasks [59, 60, 61]; *iii)* the feed-forward methods that take the hyperparameters and task datasets as input and predict the optimal model parameters [62, 63, 64]. The application of meta-learning approaches to physics problems has been mostly in the context of physics-informed neural networks (PINNs) [65] to improve their performance over a parametrized family of partial differential equations [66, 67, 68].

However, in this work, we leverage the relation between micro- and meso-scale dynamics in the response of microstructured material to external loads to propose a meta-learning framework for learning closure models at the meso-scale. Motivated by the idea of tokenization in natural language processing, we consider a meso-scale domain of microstructured material as a correlated system of interacting micro-scale building blocks. While an inner level model learns the micro-scale dynamics of each constituent independently, an outer level model “stitches” them together by learning the correlation between these micro-scale building blocks.

### 3 Method

Consider temporal partial differential equations (PDEs) of the form

$$\begin{aligned} \partial_t \mathbf{u} &= \mathcal{F}(x, \mathbf{u}, \partial_x \mathbf{u}, \partial_{xx} \mathbf{u}, \dots; \mathbf{a}), & t \in [0, \mathbb{T}], \quad x \in \mathbb{X}, \\ \mathbf{u}(0, x) &= \mathbf{u}^0(x), & x \in \mathbb{X}, \\ B[\mathbf{u}](t, x) &= 0, & t \in [0, \mathbb{T}], \quad x \in \partial\mathbb{X}, \end{aligned} \quad (3.1)$$

parametrized by a family of static parameters  $\mathbf{a}$ . The nonlinear functional  $\mathcal{F}$  in (3.1) encapsulates the governing dynamics of a system of coupled physical fields  $\mathbf{u} = (u_1, u_2, \dots, u_k) : [0, \mathbb{T}] \times \mathbb{X} \rightarrow \mathbb{R}^k$  over the spatial domain  $\mathbb{X}$  in



time interval  $[0, \mathbb{T}]$ . The notations  $\partial_x \mathbf{u}$  and  $\partial_{xx} \mathbf{u}$  denote the first-  $\frac{\partial \mathbf{u}}{\partial x}$  and second-order  $\frac{\partial^2 \mathbf{u}}{\partial x^2}$  partial derivatives w.r.t. the spatial dimension. In addition,  $\mathbf{u}^0(x)$  specifies the initial condition and  $B[\mathbf{u}](t, x) = 0$  gives the boundary conditions over the boundary  $\partial \mathbb{X}$  of the spatial domain  $\mathbb{X}$ . The parameters  $\psi = (\mathbf{a}, \partial \mathbb{X}) \in \Psi$  represent physical and geometrical properties of the system, *e.g.*, the material properties and the global shape of the boundary of the spatial domain.

By discretizing the spatial domain  $\mathbb{X}$  into a grid or mesh, the system of PDEs (3.1) leads to a parametrized dynamical system of the following form

$$\frac{d}{dt} \mathbf{U} = \tilde{\mathbf{F}}(\mathbf{U}; \psi), \quad t \in [0, \mathbb{T}], \quad \psi \in \Psi, \quad (3.2)$$

where  $\mathbf{U} = (U_1, U_2, \dots, U_k) : [0, \mathbb{T}] \rightarrow \mathbb{R}^{k \times N}$  denotes the corresponding high-dimensional *state* vector. This work employs a uniform Cartesian grid over a 2D domain  $\mathbb{X} \subset \mathbb{R}^2$ . Note that the direct numerical simulations at the micro- and meso-scales are also performed on a uniform fixed Cartesian grid [31, 29], and the data provided to the deep learning algorithms are arranged on this grid. This provides a natural connection between the evolution of the fields computed from DNS and the tessellation required for training convolutional neural networks, *i.e.*, the building blocks of the model considered in this work.

Given a dataset of consecutive time-snapshots

$$\left[ \mathbf{U}^{(t_0)}, \mathbf{U}^{(t_1)}, \dots, \mathbf{U}^{(t_n)} \right], \quad t_{j+1} - t_j = \Delta t, \quad (3.3)$$

of the state vector  $\mathbf{U}$  corresponding to various initial conditions and parameter values, we want to learn a surrogate model, which can emulate the time evolution of the dynamical system (3.2). We assume that the dominant part of the dynamics of the system happens over a lower-dimensional invariant manifold (slow manifold) embedded inside the high-dimensional input space  $\mathbb{R}^{k \times N}$  [69, 70]. Hence, we focus on learning a rich enough latent representation of the dynamical system and the corresponding evolution over the latent space.

### 3.1 Architecture Design

Our probabilistic deep learning-based model consists of two main classes of building blocks, which, roughly speaking, are responsible for

- (i) learning a nonlinear representation of the slow manifold of the system together with the most probable fluctuations of the dynamics nearby the slow manifold; and
- (ii) learning a stochastic reduced dynamics over the latent space, which captures the essence of the original dynamics in the full state space,

respectively. In order to achieve the learning task (i) in our model, we use *variational autoencoders* (VAE) [51, 71] for the compression of the high-fidelity fields  $U_i$  into corresponding latent fields  $Z_i$  which result in better generalizability and robustness of the model in sparse data regimes of the parameter space  $\Psi$  compared to the classical autoencoders. For each  $i = 1, \dots, k$ , we consider the latent field  $Z_i$  as a *discrete Gaussian random field* [72] whose two-point auto-correlation function over the spatial domain equals the identity matrix, *i.e.*,  $Z_i(x_1)$  and  $Z_i(x_2)$  are independent multivariate Gaussian random variables for all  $x_1 \neq x_2 \in \mathbb{X}$ . Hence, the latent field  $Z_i$  is uniquely determined by the two fields  $\bar{Z}_i$  and  $Z_i^\sigma$ , where  $\bar{Z}_i(x)$  and  $Z_i^\sigma(x)$  specify the mean and the log-variance of the Gaussian random variable  $Z_i(x)$ ,  $\forall x \in \mathbb{X}$ . We consider the space of pairs  $(\bar{Z}_i, Z_i^\sigma)$  of the above-mentioned form as the latent space associated with each field  $U_i$ ,  $i = 1, \dots, k$ . In other words, the latent mean fields  $\bar{Z}_i$  can be considered as elements of the slow manifold of the corresponding dynamical system, while the latent log-variance fields  $Z_i^\sigma$  capture the fluctuations of the dynamics near the slow manifold.

The encoder  $E_i = (\bar{E}_i, E_i^\sigma) : U_i \mapsto (\bar{Z}_i, Z_i^\sigma)$  of our VAE is considered to be a convolutional neural network (CNN) which encode the high-fidelity field  $U_i$  into the pair  $(\bar{Z}_i, Z_i^\sigma)$  in the following way:

$$\bar{Z}_i(x) = (\bar{K}_{\theta_i} * U_i)(x) = \int_{\mathbb{X}} \bar{K}_{\theta_i}(x - y) \cdot U_i(y) dy, \quad x \in \mathbb{X}, \quad (3.4)$$

and

$$Z_i^\sigma(x) = (K_{\theta_i}^\sigma * U_i)(x) = \int_{\mathbb{X}} K_{\theta_i}^\sigma(x - y) \cdot U_i(y) dy, \quad x \in \mathbb{X}. \quad (3.5)$$

Let  $d$  be the dimension of each latent field  $Z_i$ ,  $i = 1, \dots, k$  over the spatial domain  $\mathbb{X}$ , *i.e.*, the number of channels of the corresponding numerical tensor. In general, the convolution kernels  $\bar{K}_{\theta_i}$  and  $K_{\theta_i}^\sigma$ , in (3.4) and (3.5), can be considered as  $d$ -by-1 matrix-valued functions over  $\mathbb{X} \times \mathbb{X}$ , *i.e.*,

$$\bar{K}_{\theta_i} : \mathbb{X} \times \mathbb{X} \rightarrow \mathcal{M}_{d \times 1}(\mathbb{R}) \quad (3.6)$$

and

$$K_{\theta'_i}^\sigma : \mathbb{X} \times \mathbb{X} \rightarrow \mathcal{M}_{d \times 1}(\mathbb{R}), \quad (3.7)$$

respectively, where  $\mathcal{M}_{d \times 1}(\mathbb{R})$  denotes the set of all  $d$ -by-1 real matrices. In the particular setup of convolutional neural networks, one considers the convolution kernels to be translation-invariant matrix-valued functions with finite support, *i.e.*, a fixed-size sliding window which sweeps the spatial domain  $\mathbb{X}$ . The entries of the corresponding matrices form the set of trainable parameters  $(\theta_i, \theta'_i)$  of the corresponding models which is learned through the training process. The latent mean field  $\bar{Z}_i(x)$  (or, similarly, the log-variance field  $Z_i^\sigma(x)$ ) at each  $x \in \mathbb{X}$  is a weighted sum of  $d$ -dimensional vectors  $\bar{K}_{\theta_i}(x, y) \cdot U_i(y)$  which are result of action of the matrix  $\bar{K}_{\theta_i}(x, y)$  on the 1-dimensional vector  $U_i(y)$ ,  $\forall y \in \mathbb{X}$ .

In addition, the decoder  $D_i : Z_i \mapsto \hat{U}_i$  of our VAE is also considered to be a convolutional neural network which generate the reconstructed field  $\hat{U}_i$  in the input space from the latent field  $Z_i$  as follows:

$$\hat{U}_i(x) = (K_{\varphi_i} * Z_i)(x) = \int_{\mathbb{X}} K_{\varphi_i}(x - y) \cdot Z_i(y) dy, \quad x \in \mathbb{X}. \quad (3.8)$$

In the next step, in order to achieve the learning task (ii), the reduced dynamics (a.k.a. latent evolution) is learned through an *autoregressive* model

$$(\bar{\mathbf{Z}}, \mathbf{Z}^\sigma)_{|t_{j+1}} = \mathbf{F}_\alpha \left( (\bar{\mathbf{Z}}, \mathbf{Z}^\sigma)_{|t_j}; \psi \right), \quad \psi \in \Psi, \quad (3.9)$$

where  $\bar{\mathbf{Z}} = (\bar{Z}_1, \bar{Z}_2, \dots, \bar{Z}_k)$ ,  $\mathbf{Z}^\sigma = (Z_1^\sigma, Z_2^\sigma, \dots, Z_k^\sigma)$ , and  $\alpha$  denotes the trainable parameters of the model. In the following, we assume that all the corresponding autoregressive functionals depend on the fixed parameters  $\psi \in \Psi$  together with a set of trainable parameters  $\alpha$ , and do not mention this dependence explicitly to avoid cumbersome notation. Motivated by the Stochastic Differential Equation (SDE) framework, we decompose the dynamics induced by the mapping  $\mathbf{F}$ , in (3.9), into a *deterministic* part

$$\bar{\mathbf{Z}}_{|t_{j+1}} = \bar{\mathbf{F}}(\bar{\mathbf{Z}}_{|t_j}), \quad (3.10)$$

and a *stochastic* part

$$\mathbf{Z}_{|t_{j+1}}^\sigma = \mathbf{F}^\sigma \left( (\bar{\mathbf{Z}}, \mathbf{Z}^\sigma)_{|t_j} \right). \quad (3.11)$$

Furthermore, we decompose the mapping  $\bar{\mathbf{F}}$  representing the deterministic part of the latent evolution, *i.e.*, (3.10), in the following form

$$\bar{\mathbf{F}}(\bar{\mathbf{Z}}) = \bar{F}_{\text{corr}}(\bar{F}_{\text{dec}}(\bar{\mathbf{Z}})), \quad (3.12)$$

in which

$$\bar{F}_{\text{dec}}(\bar{\mathbf{Z}}) = \begin{bmatrix} \bar{f}_1 & & & \\ & \bar{f}_2 & & \\ & & \ddots & \\ & & & \bar{f}_k \end{bmatrix} \begin{bmatrix} \bar{Z}_1 \\ \bar{Z}_2 \\ \vdots \\ \bar{Z}_k \end{bmatrix} \quad (3.13)$$

captures the *decoupled* evolution of each latent mean-field  $\bar{Z}_i$ ,  $i = 1, \dots, k$ , independently, while  $\bar{F}_{\text{corr}}$  encapsulates the *correlation* (interaction) among all the latent mean-fields. Similarly, the mapping  $\mathbf{F}^\sigma$  representing the stochastic part of the latent evolution, *i.e.*, (3.11), is decomposed into three building blocks as the following

$$\mathbf{F}^\sigma(\bar{\mathbf{Z}}, \mathbf{Z}^\sigma) = F_{\text{corr}}^\sigma(\bar{F}_{\text{dec}}(\bar{\mathbf{Z}}), F_{\text{dec}}^\sigma(\bar{\mathbf{Z}}, \mathbf{Z}^\sigma)), \quad (3.14)$$

where  $\bar{F}_{\text{dec}}$  is given by (3.13), and

$$F_{\text{dec}}^\sigma(\bar{\mathbf{Z}}, \mathbf{Z}^\sigma) = \begin{bmatrix} f_1^\sigma & & & \\ & f_2^\sigma & & \\ & & \ddots & \\ & & & f_k^\sigma \end{bmatrix} \begin{bmatrix} (\bar{Z}_1, Z_1^\sigma) \\ (\bar{Z}_2, Z_2^\sigma) \\ \vdots \\ (\bar{Z}_k, Z_k^\sigma) \end{bmatrix}. \quad (3.15)$$

The mapping  $F_{\text{corr}}^\sigma$  in (3.14) models the correlated evolution of all the latent log-variance-fields  $Z_i^\sigma$ ,  $i = 1, \dots, k$ .

We consider a convolutional neural network [73, 74] (CNN)-based architecture for all the building blocks of our model, *i.e.*, the variational encoder, decoder, and the autoregressive functionals in (3.12) and (3.14), in order to make our model to be transferable from micro- to meso-scale. For the results presented in this paper, we consider a VGG-Net [75] and a U-Net [76] architecture for the autoencoder and the latent dynamics autoregressive functionals, respectively. It is a multi-level, multi-resolution architecture which captures the local correlation between micro-scale building blocks in a hierarchical manner. Details of the implementation are discussed in Appendix A.1. Source codes are available online at <https://github.com/ShahabAzarfar/Multiscale-Latent-Dynamics>.

### 3.2 Training

For training each VAE in our model, the corresponding trainable parameters  $(\theta_i, \theta'_i, \varphi_i)$  of the convolution kernels  $\bar{K}_{\theta_i}$ ,  $K_{\theta'_i}$  and  $K_{\varphi_i}$ , in (3.4), (3.5) and (3.8), respectively, are learned from the data by minimizing the reconstruction loss

$$\mathcal{L}_{\text{recon}} = \|U_i - \hat{U}_i\|_{L^2}^2 = \int_{\mathbb{X}} |U_i(x) - \hat{U}_i(x)|^2 dx \quad (3.16)$$

together with the Kullback-Leibler divergence loss<sup>2</sup>

$$\mathcal{L}_{\text{KL}} = \frac{1}{2} \int_{\mathbb{X}} \sum_c \left[ (\bar{Z}_{i,c}(x))^2 + \exp(Z_{i,c}^\sigma(x)) - Z_{i,c}^\sigma(x) - 1 \right] dx. \quad (3.17)$$

Note that since we are considering each latent field  $Z_i$  to be a discrete Gaussian random field with trivial two-point auto-correlation function, *i.e.*, equal to identity matrix, the Kullback-Leibler divergence loss (3.17) is essentially the Kullback-Leibler divergence between a direct sum of univariate Gaussian distributions and the standard normal distributions. We train the VAE associated with each field  $U_i$ ,  $i = 1, \dots, k$ , *independently*, and use the trained encoder to compress  $U_i$  into the corresponding latent representation  $(\bar{Z}_i, Z_i^\sigma)$ .

Let  $\mathbf{E} = (\bar{\mathbf{E}}, \mathbf{E}^\sigma) : \mathbf{U} \mapsto (\bar{\mathbf{Z}}, \mathbf{Z}^\sigma)$  and  $\mathbf{D} : \mathbf{Z} \mapsto \hat{\mathbf{U}}$  be the direct sum of the VAE-encoders and the VAE-decoders, respectively, corresponding to the fields  $U_i$ ,  $i = 1, \dots, k$ . Considering (3.9), the autoregressive rollout of our model for  $M$  time-steps can be written as

$$\tilde{\mathbf{U}}^{(t_j+M)} = \mathbf{D} \left( \mathbf{F}_\alpha(\cdot; p)^{(M)} \left( \mathbf{E} \left( \mathbf{U}^{(t_j)} \right) \right) \right) = \mathbf{D} \left( \underbrace{\mathbf{F}_\alpha(\cdot; p) \circ \dots \circ \mathbf{F}_\alpha(\cdot; p)}_{\text{composing } M \text{ times}} \left( \mathbf{E} \left( \mathbf{U}^{(t_j)} \right) \right) \right). \quad (3.18)$$

As the learning objective for training of the autoregressive model  $\mathbf{F}_\alpha(\cdot; p)$ , we consider the following three loss functions which are extensions of the loss functions introduced in [77]:

$$\mathcal{L}_{\text{multi-step}} = \sum_{m=1}^M w_m \ell \left( \mathbf{U}^{(t_j+m)}, \tilde{\mathbf{U}}^{(t_j+m)} \right), \quad (3.19)$$

$$\mathcal{L}_{\text{consistency-mean}} = \sum_{m=1}^M \frac{\|\bar{\mathbf{F}}^{(m)} \circ \bar{\mathbf{E}}(\mathbf{U}^{(t_j)}) - \bar{\mathbf{E}}(\mathbf{U}^{(t_j+m)})\|_{L^2}^2}{\|\bar{\mathbf{E}}(\mathbf{U}^{(t_j+m)})\|_{L^2}^2}, \quad (3.20)$$

and

$$\mathcal{L}_{\text{consistency-var}} = \sum_{m=1}^M \frac{\|\mathbf{F}^{\sigma(m)} \circ \mathbf{E}(\mathbf{U}^{(t_j)}) - \mathbf{E}^\sigma(\mathbf{U}^{(t_j+m)})\|_{L^2}^2}{\|\mathbf{E}^\sigma(\mathbf{U}^{(t_j+m)})\|_{L^2}^2}. \quad (3.21)$$

In (3.19), we perform  $m$ -step latent evolution and compare the reconstructed fields  $\tilde{\mathbf{U}}^{(t_j+m)}$ , given by (3.18), with the target fields  $\mathbf{U}^{(t_j+m)}$  in the *input* space, up to time horizon  $M$ . Here, the loss function  $\ell$  can typically be MSE, MAE, or  $L_2$  loss, and  $w_m$  denotes the weights for each time-step. In (3.20), we compare the  $m$ -step latent rollout of the encoded latent mean-fields  $\bar{\mathbf{F}}^{(m)} \circ \bar{\mathbf{E}}(\mathbf{U}^{(t_j)})$  with the target latent mean-field  $\bar{\mathbf{E}}(\mathbf{U}^{(t_j+m)})$  in the *latent* space. The loss function (3.21) is similar to (3.20) except the same process is applied to the latent log-variance-fields  $\mathbf{Z}^\sigma$  instead of the latent mean-fields  $\bar{\mathbf{Z}}$ .

## 4 Results

The thermomechanics governing the evolution of physical fields over a meso-scale domain (*i.e.*, size of  $O(100 \mu\text{m})$ ) of shock-loaded porous EM is the result of complex interactions between micro-scale dynamics resulting from the collapse of individual pores [1]. The full set of governing equations for the corresponding dynamics is given as a system of hyperbolic PDEs, which involves the conservation laws for mass, momentum, and energy together with appropriate constitutive models such as the equation of state and flow rules. It describes the temporal evolution of a set of coupled physical fields, including the density, temperature, and pressure scalar fields; the velocity vector field; and the stress and strain 2-tensor fields (see [78, 26, 79] for details). The direct numerical simulation (DNS) data used in this paper

<sup>2</sup>The  $c$ -th component of the vectors  $\bar{Z}_i(x)$  and  $Z_i^\sigma(x)$  are denoted by  $\bar{Z}_{i,c}(x)$  and  $Z_{i,c}^\sigma(x)$ , respectively.

is generated by solving the above-mentioned full system of coupled PDEs. More details on the numerical simulation setup are provided in Appendix A.2. In this work, following [17], we consider the dynamical system corresponding to the evolution of the temperature  $T$ , pressure  $P$  and microstructural morphology  $\mu$  fields which are more directly related to the evolution of hotspots to quantify energy localization at the meso-scale to determine the macro-scale shock sensitivity quantities of interest for EM [80]. These three fields play key roles in so-called reactive burn models which are commonly used to drive shock-to-detonation calculations in production hydrocodes [81]. Our goal is to learn a surrogate model for the coupled dynamics of these three fields over a meso-scale domain in EM microstructures.

We follow a *meta-learning* approach to leverage a relatively large dataset of inexpensive micro-scale simulations, corresponding to single-pore collapse, combined with a small dataset of meso-scale simulations for the above-mentioned learning process. The proposed meta-learning framework is based on the idea that the meso-scale dynamics can be considered as a correlated system of interacting micro-scale building blocks, where the constituents can be learned from the underlying micro-scale physics. In this approach, we start by learning a latent representation of the micro-scale dynamics from a relatively large dataset ( $O(100)$  samples) of micro-scale single pore collapse simulations. These machine-learned latent representations are considered as the building blocks of a “first order approximation” of the meso-scale dynamics. In the next step, in order to learn the “higher order corrections” corresponding to the correlation between the micro-scale building blocks, we train our model over a relatively small ( $< 10$  samples) dataset of meso-scale simulations. We elaborate on the above-mentioned two steps of our proposed meta-learning framework in Section 4.1 and 4.2, respectively.

#### 4.1 Learning a latent representation of micro-scale dynamics

In this section, we describe the learning process of a reduced representation of the micro-scale dynamics of the coupled fields  $T$ ,  $P$  and  $\mu$  corresponding to the shock-induced deformation in a 2D-domain of porous energetic material containing an isolated single-void (see Figure 1 (a)). We consider a probabilistic deep learning-based model following the architecture discussed in Section 3.1.

We start by learning a nonlinear representation of the slow manifold of the system. To this end, we train three independent VAEs, associated with  $T$ ,  $P$ , and  $\mu$  fields, on the single-void data in order to construct latent representations of the form  $(\bar{Z}_T, Z_T^\sigma)$ ,  $(\bar{Z}_P, Z_P^\sigma)$  and  $(\bar{Z}_\mu, Z_\mu^\sigma)$ , respectively. A visual 3D-embedding of the slow manifold of temperature latent mean fields  $\bar{Z}_T$ , corresponding to the hotspot ignition and growth due to shock-induced single pore collapse in EM, is shown in Figure 2.<sup>3</sup> One can see that the latent mean fields  $\bar{Z}_T$  are initially quite close to each other which reflects the fact that, starting from the constant initial condition  $T = 300\text{K}$ , the temperature fields of all sample simulations, corresponding to the collapse of voids with various sizes and shapes, remain quite similar before the arrival of the shock front at the void which initiates the void-collapse and formation of hotspots. However, in later time-steps, the corresponding slow manifold expands and bifurcates into several branches depending on the temperature distribution and growth of the resulting hotspot.

In the next step, we want to learn the stochastic reduced dynamics of the encoded latent fields  $(\bar{Z}_U, Z_U^\sigma)$ , where  $U$  denotes one of the physical fields  $T, P, \mu$ . Considering (3.12) and (3.14), it consists of learning the decoupled latent evolution mappings  $(\bar{F}_{\text{dec}}, F_{\text{dec}}^\sigma)$ , given by (3.13) and (3.15), in addition to the field-correlation mappings  $(\bar{F}_{\text{corr}}, F_{\text{corr}}^\sigma)$ . We start by learning the decoupled evolution of each latent field  $(\bar{Z}_U, Z_U^\sigma)$ , given by the associated autoregressive functionals  $(\bar{f}_U, f_U^\sigma)$ , independently, where  $U = T, P, \mu$ . A schematic diagram of the decoupled latent evolution models, along with the corresponding variational encoder and decoder, is illustrated in Figure 3. The loss functions for training of each  $(\bar{f}_U, f_U^\sigma)$  are the same loss functions  $\mathcal{L}_{\text{multi-step}}$ ,  $\mathcal{L}_{\text{consistency-mean}}$  and  $\mathcal{L}_{\text{consistency-var}}$ , given by (3.19), (3.20) and (3.21), respectively, in the case of a single field  $U$ . The direct sum of the learned decoupled latent evolution models  $(\bar{f}_U, f_U^\sigma)$ , for  $U = T, P, \mu$ , is considered as  $(\bar{F}_{\text{dec}}, F_{\text{dec}}^\sigma)$ .

We notice that the decoupled latent evolution models can only encapsulate the *local* behavior of the underlying dynamical system corresponding to the evolution of temperature  $T$ , pressure  $P$ , and microstructural morphology  $\mu$  fields. For example, although the short rollout of the autoregressive mapping  $(\bar{f}_T, f_T^\sigma)$  can capture, to some extent, the advection and diffusion of a hotspot after its formation, its long rollout starting from  $t = 0$  can hardly make any stable prediction of the temperature evolution. Hence, it is of fundamental importance to learn the mutual correlation and interaction between the three evolving physical fields  $T, P$  and  $\mu$  which is captured by the latent evolution mapping  $(\bar{F}_{\text{corr}}, F_{\text{corr}}^\sigma)$ .

We consider the full autoregressive functional as the composition of  $(\bar{F}_{\text{corr}}, F_{\text{corr}}^\sigma)$  with  $(\bar{F}_{\text{dec}}, F_{\text{dec}}^\sigma)$  according to (3.12) and (3.14). The deterministic part of the correlated dynamics of the latent mean fields  $\bar{Z}_T$ ,  $\bar{Z}_P$  and  $\bar{Z}_\mu$  is learned by the

<sup>3</sup>We used a nonlinear dimensionality reduction technique, called PHATE [82], for visualizing the manifold embedding. It is based on the Diffusion Maps algorithm [83] which defines an intrinsic notion of distance between the data points.

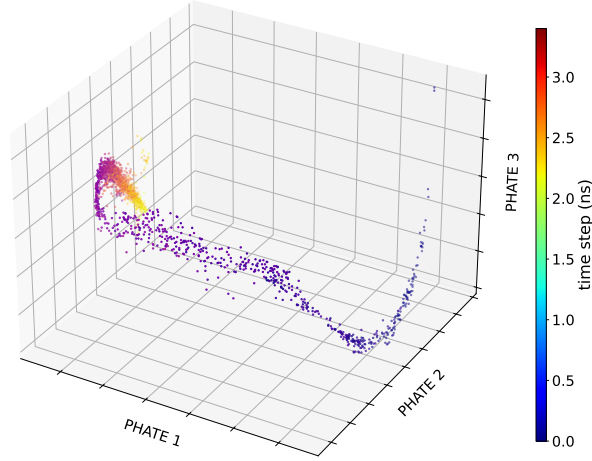
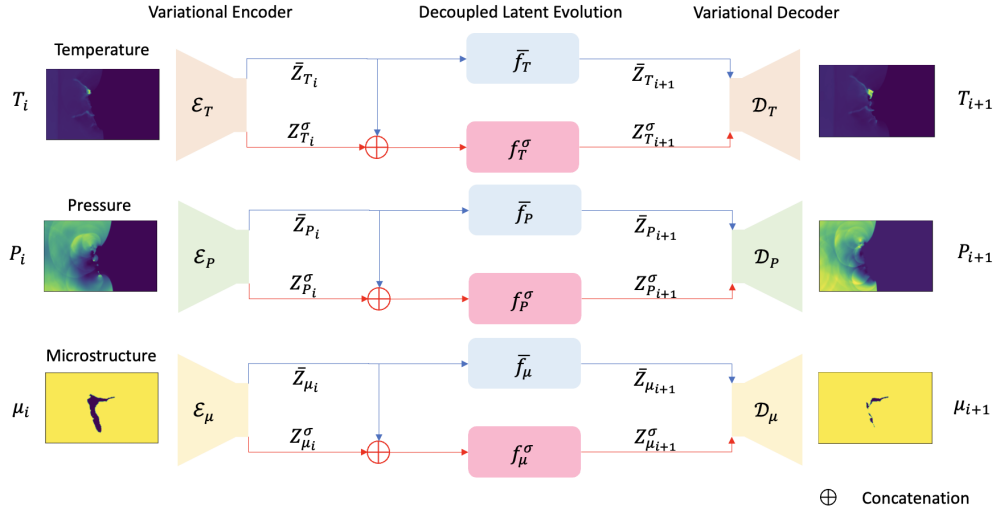
Figure 2: 3D visualization of the slow manifold of temperature latent mean fields  $\bar{Z}_T(t)$ 

Figure 3: Schematic diagram of the decoupled latent evolution model

mapping  $\bar{F}_{\text{corr}}$ . On the other hand, the mapping  $F_{\text{corr}}^\sigma$  encapsulates the inherent stochasticity in the coupled evolution of all the corresponding latent fields  $(\bar{Z}_U, Z_U^\sigma)$  for  $U = T, P, \mu$ . A detailed illustration of the way in which various building blocks of the latent autoregressive functionals and the three variational autoencoders are combined to construct our full model is given in Figure 4.

The composition of  $(\bar{F}_{\text{corr}}, F_{\text{corr}}^\sigma)$  with  $(\bar{F}_{\text{dec}}, F_{\text{dec}}^\sigma)$  makes our model capable of learning the *global*, in addition to the local, dynamics of the underlying coupled physical fields. In other words, starting from the initial condition for the temperature  $T$ , pressure  $P$  and microstructural morphology  $\mu$  fields at  $t = 0$ , the long-time rollout of the full autoregressive model can predict the evolution of all three fields with reasonable accuracy. Note that the coupled dynamics of these fields involves, at least, two quite distinct phases [84, 85]: i) hotspot-ignition phase: the time period up to complete collapse of voids which results in ignition and formation of high temperature regions called hotspots; ii) hotspot-growth phase: the time period in which the highly intense energy localized in the hotspots start to diffuse through the energetic material. The “kinks” in the slow manifold of  $\bar{Z}_T$ , illustrated in Figure 2, can be interpreted as the transition point between these different phases of the underlying dynamics. The existence of these “phase transitions” makes learning the long-term (global) dynamics of the coupled fields  $T$ ,  $P$ , and  $\mu$ , a challenging task.

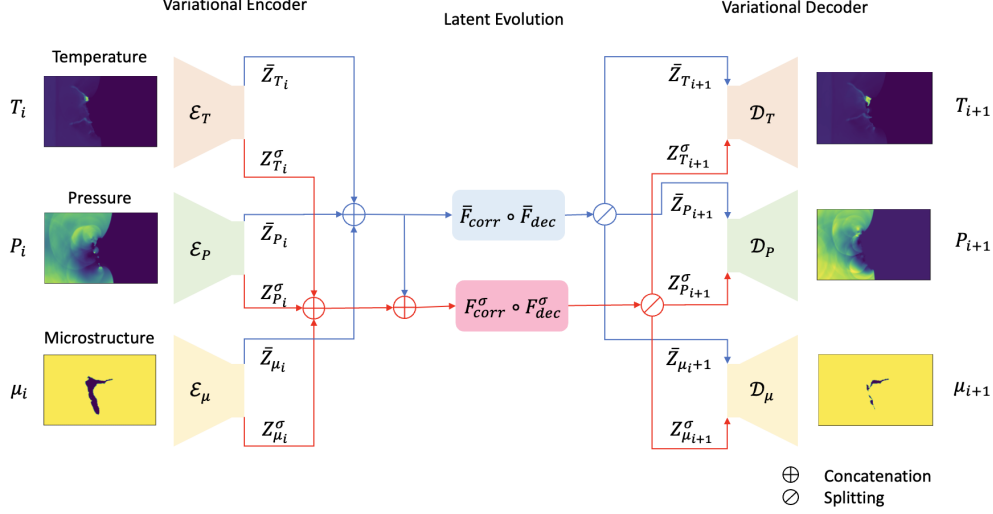


Figure 4: Schematic diagram of the combination of three VAEs with the autoregressive latent evolution mappings in our full model.

A direct numerical simulation of the evolution of the temperature  $T$  and pressure  $P$  fields generated by shock-induced single pore collapse followed by hotspot ignition and growth, is illustrated in the top rows of Figure 5 (a) and (b), respectively. Roughly speaking, the time-periods  $t \in [0, 1.03 \text{ ns}]$  and  $t \in [1.03 \text{ ns}, 2.75 \text{ ns}]$  represent the above-mentioned two phases of the underlying dynamics, *i.e.*, the ignition and the hotspot growth phases, respectively. The second rows of these figures show the global dynamics of the predicted temperature  $\hat{T}$  and pressure field  $\hat{P}$ , respectively, resulting from the long-term rollout of our autoregressive model, given the initial condition of  $T, P, \mu$  at  $t = 0$ . Recall that, in our full model, the predicted temperature field  $\hat{T}$  (resp. predicted pressure field  $\hat{P}$ ) is reconstructed by the temperature variational decoder  $D_T$  (resp. pressure variational decoder  $D_P$ ) from the evolved temperature latent mean field  $\bar{Z}_T$  and the temperature latent log-variance field  $Z_T^\sigma$  (resp. pressure latent mean field  $\bar{Z}_P$  and the pressure latent log-variance field  $Z_P^\sigma$ ).

In this work, we consider each of the latent mean field  $\bar{Z}_U$  and the latent log-variance field  $Z_U^\sigma$ ,  $U = T, P, \mu$ , as a four-dimensional field over the underlying spatial domain  $\mathbb{X}$ , *i.e.*,

$$\bar{Z}_U = (\bar{Z}_{U,1}, \bar{Z}_{U,2}, \bar{Z}_{U,3}, \bar{Z}_{U,4}) \quad (4.1)$$

and

$$Z_U^\sigma = (Z_{U,1}^\sigma, Z_{U,2}^\sigma, Z_{U,3}^\sigma, Z_{U,4}^\sigma), \quad (4.2)$$

where each of  $\bar{Z}_{U,j}$  and  $Z_{U,j}^\sigma$ ,  $j = 1, \dots, 4$ , denotes a scalar field over  $\mathbb{X}$ . In other words, each latent field  $Z_U$  is considered to be a discrete Gaussian random field over  $\mathbb{X}$ , where, for each  $x \in \mathbb{X}$ ,  $Z_U(x)$  is a four-dimensional Gaussian random variable.<sup>4</sup> Figure 6 (a) and (b) illustrate the evolution of the dominant component among the four components of  $(\bar{Z}_T, Z_T^\sigma)$  and  $(\bar{Z}_P, Z_P^\sigma)$ , respectively. Here, we have considered a pair of scalar fields  $(\bar{Z}_{T,j}, Z_{T,j}^\sigma)$  (resp.  $(\bar{Z}_{P,j}, Z_{P,j}^\sigma)$ ) as a dominant component if it captures the evolution of most of the features which are fundamental for reconstructing the corresponding field  $T$  (resp.  $P$ ) in the input space. Note that the dominant components  $(\bar{Z}_{T,4}, Z_{T,4}^\sigma)$  and  $(\bar{Z}_{P,2}, Z_{P,2}^\sigma)$  of the temperature and pressure latent field, respectively, involve patterns induced from *all* the three coupled fields: temperature  $T$ , pressure  $P$  and microstructural morphology  $\mu$ . This fact highlights the importance of the correlation autoregressive functional  $\bar{F}_{\text{corr}}$ , which *intertwines* the dominant features from all the three coupled fields that are essential for learning the underlying *global* dynamics.

## 4.2 Learning the correlation between micro-scale building blocks

Following our proposed meta-learning framework, we consider the micro-scale latent fields  $(\bar{Z}_T, Z_T^\sigma)$ ,  $(\bar{Z}_P, Z_P^\sigma)$  and  $(\bar{Z}_\mu, Z_\mu^\sigma)$ , whose learning process is described in Section 4.1, as the building blocks of meso-scale dynamics of the coupled fields  $(T, P, \mu)$ . In this section, we describe how this micro-scale information is leveraged to learn the

<sup>4</sup>Using the notation introduced in (3.6) and (3.7), we have considered  $d = 4$ . Note that the choice of the dimension of the latent field can vary depending on the considered dataset and the chosen neural network architecture of the VAE.

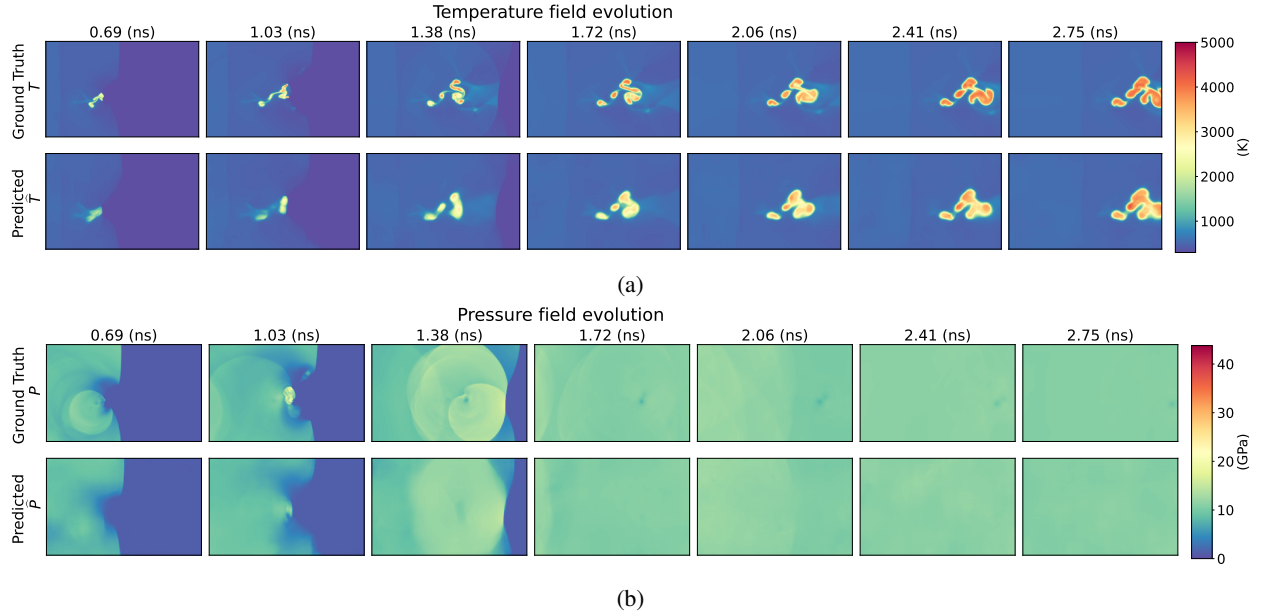


Figure 5: Our model’s prediction of the (a) temperature and (b) pressure field evolution corresponding to shock-induced single-pore collapse in EM.

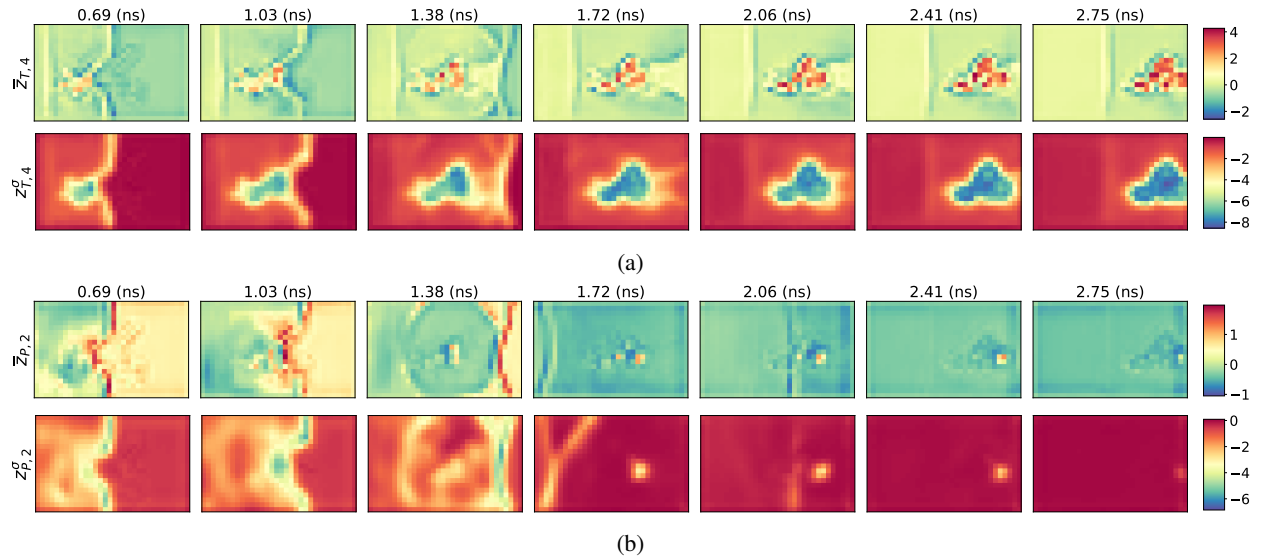


Figure 6: Evolution of latent mean and latent log-variance fields. (a) dominant latent field in the prediction of the temperature field  $T$ . (b) dominant latent field in the prediction of the pressure field  $P$ .

corresponding meso-scale dynamics by training our “micro-scale-learned” model using a relatively small dataset of meso-scale simulations.

Let  $\mathbb{X}_{\text{mes}}$  denote a meso-scale domain of porous energetic material consisting of a field of voids. Consider the parametrized dynamical system

$$\frac{d}{dt}\mathbf{U} = \tilde{\mathbf{F}}_{\text{mes}}(\mathbf{U}; \psi), \quad \psi \in \Psi, \quad (4.3)$$

corresponding to the evolution of the state vector  $\mathbf{U} = (T, P, \mu)$ , where the parameters  $\psi \in \Psi$  represent the geometrical and morphological characteristics of the underlying domain  $\mathbb{X}_{\text{mes}}$  at  $t = 0$ .<sup>5</sup> It is known that, depending on the geometrical properties of the underlying field of voids, the patterns of the temperature  $T$  and pressure  $P$  fields and their evolution, during the hotspot ignition and growth, can be quite different. In other words, the global behavior of the dynamical system (4.3) can change considerably by varying the geometric parameters  $\psi$ . In the following, we assume that the parametric solution map  $\psi \mapsto \mathbf{U}_{\text{mes}}(t; \psi)$  is a well-defined mapping from a low-dimensional manifold in the parameter space  $\Psi$  to an appropriate function space over the time-interval  $[0, \mathbb{T}]$ . In addition, we suppose that the meso-scale microstructures are sampled from a probability distribution  $\mathcal{P}(\psi)$  over the parameter space  $\Psi$ . Using the parametric solution map  $\psi \mapsto \mathbf{U}_{\text{mes}}(\cdot; \psi)$ , one can push-forward  $\mathcal{P}(\psi)$  to the corresponding function space in order to get a stochastic process  $\{\mathbf{U}_{\text{mes}}(t)\}_{t \in [0, \mathbb{T}]}$  over the state space of the dynamical system (4.3). We use our probabilistic model to learn the underlying dynamics corresponding to this stochastic process.

Let  $\{\mathbf{Z}_{\text{mes}}(t)\}_{t \in [0, \mathbb{T}]}$  be the stochastic process over the latent space, where  $\mathbf{Z}_{\text{mes}}(t)$  denotes the direct sum of the Gaussian random fields encoded by the variational encoders for the temperature  $T$ , pressure  $P$  and microstructural morphology  $\mu$  fields, respectively. According to the Bayes’ theorem, the marginal probability distributions of the two stochastic processes  $\{\mathbf{U}_{\text{mes}}(t)\}_{t \in [0, \mathbb{T}]}$  and  $\{\mathbf{Z}_{\text{mes}}(t)\}_{t \in [0, \mathbb{T}]}$  satisfy

$$\mathcal{P}(\mathbf{Z}_{\text{mes}}(t) | \mathbf{U}_{\text{mes}}(t)) \mathcal{P}(\mathbf{U}_{\text{mes}}(t)) = \mathcal{P}(\mathbf{U}_{\text{mes}}(t) | \mathbf{Z}_{\text{mes}}(t)) \mathcal{P}(\mathbf{Z}_{\text{mes}}(t)). \quad (4.4)$$

at each  $t \in [0, \mathbb{T}]$ . The two conditional probability distributions  $\mathcal{P}(\mathbf{Z}_{\text{mes}}(t) | \mathbf{U}_{\text{mes}}(t))$  and  $\mathcal{P}(\mathbf{U}_{\text{mes}}(t) | \mathbf{Z}_{\text{mes}}(t))$ , in (4.4), are approximated by the variational encoder and decoder of our model, respectively. In other words, we use the pre-trained variational autoencoders on the micro-scale data, while their trainable parameters are kept frozen, to encode the input field  $\mathbf{U}_{\text{mes}}$  into the corresponding latent mean field  $\bar{\mathbf{Z}}_{\text{mes}}$  and latent log-variance field  $\mathbf{Z}_{\text{mes}}^\sigma$ , and decode back into the input space. Hence, in order to learn the evolution of the state vector  $\mathbf{U}_{\text{mes}} = (T, P, \mu)$  corresponding to a meso-scale domain, it suffices to learn the dynamics of the latent Gaussian random field  $\mathbf{Z}_{\text{mes}}(t)$ .

We consider  $\{\mathbf{Z}_{\text{mes}}(t)\}_{t \in [0, \mathbb{T}]}$  as a Markov process whose transition operator  $\hat{\mathbf{F}}_{\text{mes}}$  describes the evolution of the corresponding marginal probability distribution, *i.e.*,

$$\mathcal{P}(\mathbf{Z}_{|t_{j+1}}) = \hat{\mathbf{F}}_{\text{mes}} \mathcal{P}(\mathbf{Z}_{|t_j}). \quad (4.5)$$

In addition, since  $\mathbf{Z}_{\text{mes}}(t)$  is considered to be a discrete Gaussian random field with trivial auto-correlation function with respect to the underlying spatial coordinate, the Markov transition operator  $\hat{\mathbf{F}}_{\text{mes}}$  can be reformulated in terms of an autoregressive functional  $\mathbf{F}_{\text{mes}}$  acting on the corresponding mean and log-variance fields in the following form

$$(\bar{\mathbf{Z}}, \mathbf{Z}^\sigma)_{|t_{j+1}} = \mathbf{F}_{\text{mes}} \left( (\bar{\mathbf{Z}}, \mathbf{Z}^\sigma)_{|t_j} \right), \quad (4.6)$$

as mentioned in (3.9). The detailed way in which  $\mathbf{F}_{\text{mes}}$  acts on each component of  $\bar{\mathbf{Z}}$  and  $\mathbf{Z}^\sigma$  is described in Equations (3.10) - (3.15). We formulate the problem of learning the autoregressive functional  $\mathbf{F}_{\text{mes}}$  in a meta-learning framework in the following.

As discussed before, generating the simulation data for the evolution of the state vector  $\mathbf{U} = (T, P, \mu)$  in the case of micro-scale single pore collapse is much cheaper than the corresponding meso-scale simulation. Hence, in the first step, we learn the micro-scale autoregressive functional  $\mathbf{F}_{\text{mic}}$  over a relatively large dataset of single-void collapse simulations. The functional  $\mathbf{F}_{\text{mic}}$  captures the coupled evolution of the temperature  $T$ , pressure  $P$  and microstructural morphology  $\mu$  fields in a micro-scale domain. We consider  $\mathbf{F}_{\text{mic}}$  as a “first-order approximation” of the meso-scale autoregressive functional  $\mathbf{F}_{\text{mes}}$  in the following sense. Motivated by tokenization in Natural Language Processing (NLP), suppose the meso-scale domain  $\mathbb{X}_{\text{mes}}$  can be decomposed into a disjoint union of micro-scale domains  $\mathbb{X}_{\text{mic}}^i$ ,  $i \in I$ , as

$$\mathbb{X}_{\text{mes}} = \bigsqcup_{i \in I} \mathbb{X}_{\text{mic}}^i, \quad (4.7)$$

<sup>5</sup>In this work, we restrict ourselves to the case of a fixed energetic material. Hence, the variations between the chemical properties of various energetic material is beyond the scope of this work.



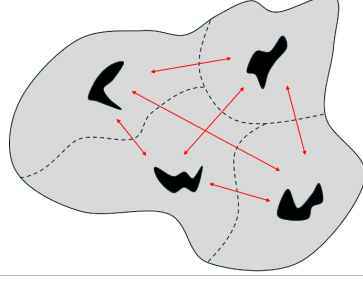


Figure 7: Division of a meso-scale domain  $\mathbb{X}_{\text{mes}}$  into micro-scale subdomains  $\mathbb{X}_{\text{mic}}^i$ : void-void interaction at the meso-scale

in such a way that the morphological characteristics of each micro-scale domain  $\mathbb{X}_{\text{mic}}^i$  is represented by a parameter  $\psi^i \in \Psi$  in the parameter space  $\Psi$ . For each micro-scale domain  $\mathbb{X}_{\text{mic}}^i$ ,  $i \in I$ , let  $\mathbf{U}_{\text{mic}}^i$  be the evolution of the state vector  $\mathbf{U} = (T, P, \mu)$  over  $\mathbb{X}_{\text{mic}}^i$  which is predicted by the micro-scale trained model  $\mathbf{F}_{\text{mic}}$  given the data  $(\mathbb{X}_{\text{mic}}^i, \psi^i)$ . After applying the appropriate time-delay necessary for the shock wave propagation over a meso-scale domain, the direct sum of the predicted micro-scale evolutions  $\mathbf{U}_{\text{mic}}^i$  might be considered as a rough approximation of  $\mathbf{U}_{\text{mes}}$  for a very short period of time-span. However, it is known that the interaction between different voids in a meso-scale domain play a crucial role in the long time-span of meso-scale dynamics  $\mathbf{U}_{\text{mes}}$ . Hence, our micro-scale autoregressive model  $\mathbf{F}_{\text{mic}}$  needs to learn the correlation between the micro-scale building blocks of the underlying meso-scale dynamics  $\mathbf{U}_{\text{mes}}$  in order to capture the fundamental effects of void-void interaction at meso-scale. In other words, one can consider

$$\mathbf{F}_{\text{mes}} = \mathbf{F}_{\text{mic}} + \text{“higher-order correction terms”} \quad (4.8)$$

where the correction terms capture the mutual interaction between the dynamics of neighboring micro-scale latent fields.

The problem of solving a parametrized family of PDEs can be seen through the lens of meta-learning as discussed in [55]. In this setup, one considers learning the PDE solution corresponding to each region of the parameter space over which the mathematical characteristics of the PDE remain the same, *e.g.*, the Navier-Stokes equation with specific Reynolds number range, as a *task*. Hence, learning the PDE solution corresponding to the non-overlapping subsets of the full parameter space can be considered as a family of closely related tasks which one aims to extract common meta information from them. Similarly, we consider the problem of learning the micro-scale dynamics  $\mathbf{F}_{\text{mic}}$  of the state vector  $\mathbf{U} = (T, P, \mu)$  corresponding to the collapse of single-voids with various morphological characteristics  $\psi \in \Psi$  as a family of correlated tasks. The common knowledge extracted from this family of tasks gives a short-term approximation of the dynamics over each micro-scale domain  $\mathbb{X}_{\text{mic}}^i$ . We use this fundamental information by transferring our micro-scale trained model to a meso-scale domain, and using its learned parameters as the initial-value for the trainable parameters of the meso-scale dynamics model  $\mathbf{F}_{\text{mes}}$ .

As mentioned before, we consider a fully convolutional, *i.e.*, CNN-based, architecture for the autoregressive mapping in our model which enables us to transfer the model from micro- to meso-scale. Let  $\bar{\mathbf{L}}_{\theta}$  and  $\mathbf{L}_{\theta'}^{\sigma}$  be the convolution kernels corresponding to the deterministic  $\bar{\mathbf{F}}$  and stochastic  $\mathbf{F}^{\sigma}$  parts of the latent evolution model given by (3.10) and (3.11), respectively. That is

$$\begin{aligned} \bar{\mathbf{Z}}_{|t_{j+1}}(x) &= \bar{\mathbf{F}}(\bar{\mathbf{Z}}_{|t_j})(x) \\ &= (\bar{\mathbf{L}}_{\theta} * \bar{\mathbf{Z}}_{|t_j})(x) \\ &= \int_{\mathbb{X}_{\text{mes}}} \bar{\mathbf{L}}_{\theta}(x-y) \cdot \bar{\mathbf{Z}}_{|t_j}(y) dy, \quad x \in \mathbb{X}_{\text{mes}}, \end{aligned} \quad (4.9)$$

and

$$\begin{aligned} \mathbf{Z}_{|t_{j+1}}^{\sigma}(x) &= \mathbf{F}^{\sigma}((\bar{\mathbf{Z}} \oplus \mathbf{Z}^{\sigma})_{|t_j})(x) \\ &= (\mathbf{L}_{\theta'}^{\sigma} * (\bar{\mathbf{Z}} \oplus \mathbf{Z}^{\sigma})_{|t_j})(x) \\ &= \int_{\mathbb{X}_{\text{mes}}} \mathbf{L}_{\theta'}^{\sigma}(x-y) \cdot (\bar{\mathbf{Z}} \oplus \mathbf{Z}^{\sigma})_{|t_j}(y) dy, \quad x \in \mathbb{X}_{\text{mes}}. \end{aligned} \quad (4.10)$$

Considering the notation introduced in (3.6) and (3.7), the convolution kernels  $\bar{\mathbf{L}}_{\theta}$  and  $\mathbf{L}_{\theta'}^{\sigma}$  can be considered as matrix-valued functions defined over the meso-scale domain  $\mathbb{X}_{\text{mes}}$  with values in  $\mathcal{M}_{d \times d}$  and  $\mathcal{M}_{d \times 2d}$ , respectively. We

start the learning process of the trainable parameters  $(\theta, \theta')$  of the convolution kernels  $\bar{\mathbf{L}}_\theta$  and  $\mathbf{L}_{\theta'}^\sigma$  by training our model on a relatively large dataset of inexpensive micro-scale simulations. After the model learns a latent representation of the micro-scale dynamics, we transfer it and train it on a small dataset of meso-scale simulations in order to learn the correlations between neighboring micro-scale building blocks of the meso-scale dynamics. In other words, the learned parameters  $(\theta, \theta')_{\text{mic}}$  at the micro-scale are considered as the initialization of the meso-scale model's parameters  $(\theta, \theta')_{\text{mes}}$ , and they will be updated as the model learns the higher-order corrections mentioned in (4.8). Roughly speaking, the transition from the initial parameters  $(\theta, \theta')_{\text{mic}}$  to  $(\theta, \theta')_{\text{mes}}$  in our model can be considered as a way of “stitching” the micro-scale dynamics over neighboring micro-scale domains  $\mathbb{X}_{\text{mic}}^i$  using the convolutional formulation of the latent evolution autoregressive functional  $\mathbf{F}_{\text{mes}}$ . Considering our CNN-based architecture, the above-mentioned higher-order corrections take into account the effects of short-range void-void interaction in each *local* neighborhood of  $\mathbb{X}_{\text{mes}}$  which is covered by the *receptive field* [86] of the convolution kernels  $\bar{\mathbf{L}}_\theta$  and  $\mathbf{L}_{\theta'}^\sigma$ .<sup>6</sup>

Figure 8 (a) illustrates the progressive improvement in the predicted meso-scale temperature evolution as the latent autoregressive model undergoes a transition from  $\mathbf{F}_{\text{mic}}$  to  $\mathbf{F}_{\text{mes}}$ . The first row shows the ground-truth, and the second row corresponds to the predicted evolution by the micro-scale-trained autoregressive functional  $\mathbf{F}_{\text{mic}}$  before learning the mutual interaction between the dynamics of neighboring micro-scale building blocks. The third up to the fifth row illustrate the predicted evolution by  $\mathbf{F}_{\text{mes}}$  after training for 50, 500, and 1,000 epochs, respectively, over the meso-scale dataset. It can be seen that the deviation between the ground-truth and the  $\mathbf{F}_{\text{mic}}$ -predicted temperature evolution becomes more considerable for longer time spans. This observation is consistent with our hypothesis in which we consider the direct sum of the latent representation of the micro-scale dynamics to approximate the meso-scale dynamics *only* over a very short time-period. After only 50 epochs of training over meso-scale dataset, the updated model is able to capture the main features of the global dynamics at the meso-scale in terms of the overall pattern of hotspots in addition to the propagation of the shock-front. However, there is a considerable false-positive predicted ignition after 50 epochs of training, which is mainly due to the fact that all the micro-scale single-pore collapse cases seen by the model has led to hotspot ignition, which is not the case at the meso-scale. As the training over the meso-scale dataset continues, *i.e.*, after 500 and 1000 epochs, the prediction performance of the meso-scale model  $\mathbf{F}_{\text{mes}}$  improves by learning the higher-order corrections which capture the correlation between neighboring micro-scale building blocks.

In order to highlight the crucial role played by the first step in our two-step meta-learning framework, *i.e.*, learning  $\mathbf{F}_{\text{mic}}$  as a “first order approximation” of  $\mathbf{F}_{\text{mes}}$ , we also consider a setup in which the meso-scale autoregressive functional  $\mathbf{F}_{\text{mes}}$  is trained from *scratch* over the same meso-scale dataset considered above. In other words, instead of considering the micro-scale-learned parameters  $(\theta, \theta')_{\text{mic}}$  as the initial value for  $(\theta, \theta')_{\text{mes}}$ , the trainable parameters  $(\theta, \theta')_{\text{mes}}$  of the meso-scale autoregressive functional  $\mathbf{F}_{\text{mes}}$  gets initialized randomly. The second up to the fourth row of Figure 8 (b) illustrate the predicted temperature evolution by  $\mathbf{F}_{\text{mes}}$  after training for 50, 500, and 1,000 epochs, respectively, from scratch. One can see that, even after 1000 epochs of training  $\mathbf{F}_{\text{mes}}$  from scratch, the model prediction misses a considerable portion of hotspot ignition and growth compared to the ground-truth.

### 4.3 Comparison with a Physics-aware Recurrent Convolutional neural network (PARC) in scarce meso-scale data regime

In this section, we compare the prediction performance of our model with a Physics-aware Recurrent Convolutional neural network (PARC) [17, 87] in a scarce meso-scale data regime. The choice of PARC, among other Physics-Informed Machine Learning (PIML) [16] models, is motivated by the underlying *inductive bias* considered in its architecture design which is particularly suited for learning fast and transient spatiotemporal dynamics with sharp gradients (see [87] for comparison between prediction performance of PARCv2 and other PIML models in the case of micro-scale single-pore collapse in EM).<sup>7</sup> PARC has a differentiator-integrator architecture, which learns the evolution of physical fields represented by a dynamical system of the form

$$\frac{d}{dt}\mathbf{U} = \tilde{\mathbf{F}}(\mathbf{U}; \psi), \quad t \in [0, T], \quad \psi \in \Psi. \quad (4.11)$$

The differentiator module aims to learn the infinitesimal evolution of the corresponding physical fields encapsulated into  $\tilde{\mathbf{F}}$  while the integrator module computes  $\Delta\mathbf{U}$  between two consecutive time-steps  $[t_i, t_i + \Delta t]$ . The integrator module is considered to be a classical numerical integrator, *e.g.*, Runge-Kutta methods, together with a neural network learning the higher-order corrections. In addition, to better capture the advection-dominant phenomenon, the PARCv2

<sup>6</sup>The notion of receptive field of convolutional neural networks is a important characteristic of CNNs which represent the pixel domain in the input image which affects the value of each output pixel, and the area outside of the receptive field has no contribution to the corresponding output pixel. Mathematically, it is equivalent to the notion of *support* of the function  $\bar{\mathbf{L}}_\theta(x, y)$  (or  $\mathbf{L}_{\theta'}^\sigma(x, y)$ ) for each fixed  $x \in \mathbb{X}_{\text{mes}}$ , which is defined as the set of  $y \in \mathbb{X}_{\text{mes}}$  for which  $\bar{\mathbf{L}}_\theta(x, y) \neq 0$ .

<sup>7</sup>Note that because of lack of a closed system of PDEs governing the evolution of the physical fields  $(T, P)$  in shock-induced energy localization in EMs, the PIML models which are based on the *learning bias* approach are not applicable to this problem.

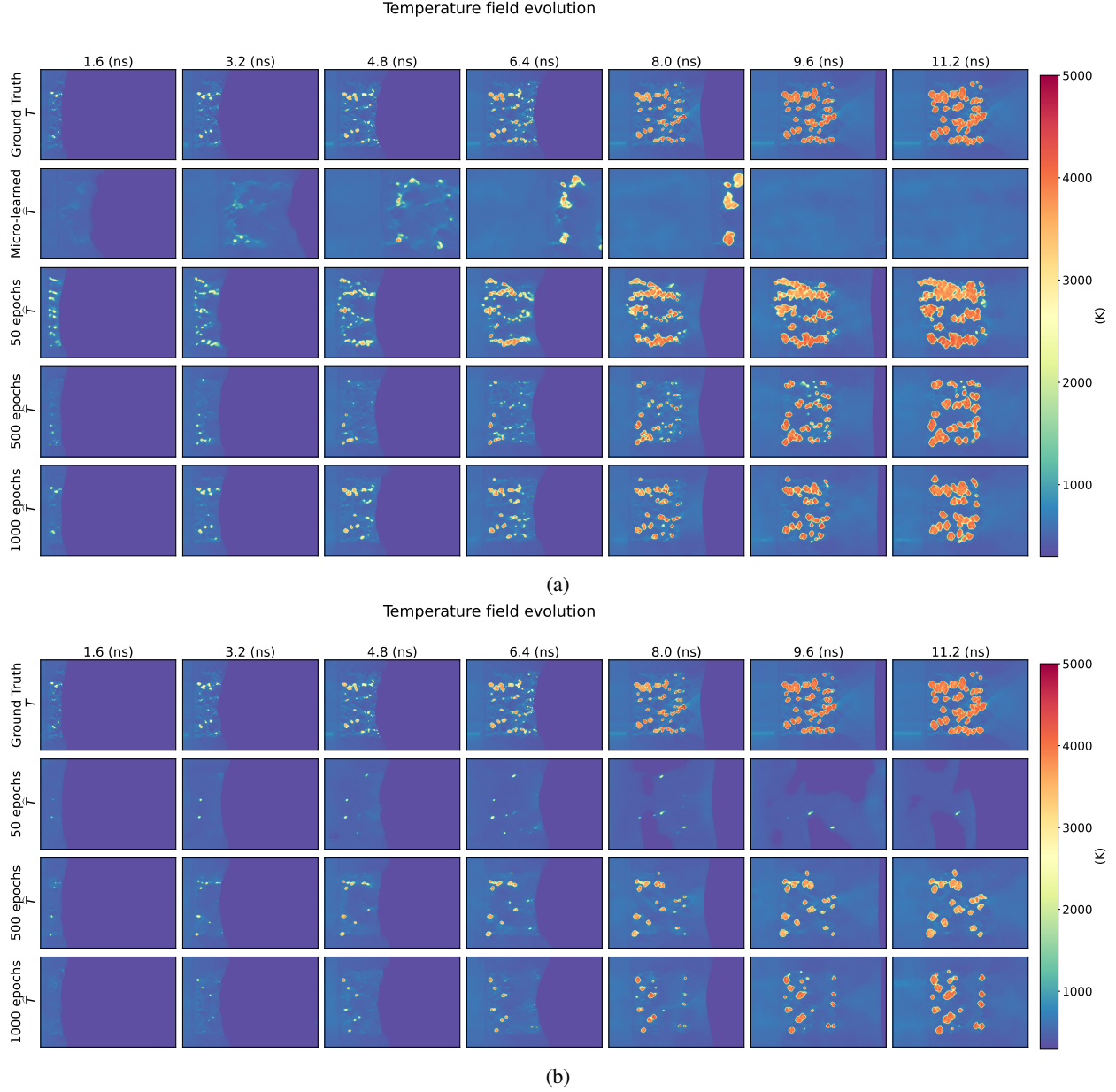


Figure 8: Predicted meso-scale temperature evolution corresponding to progressive training of meso-scale autoregressive functional  $F_{mes}$  (a) initialized from micro-scale-learned model  $F_{mic}$  (b) initialized with random weights from scratch.

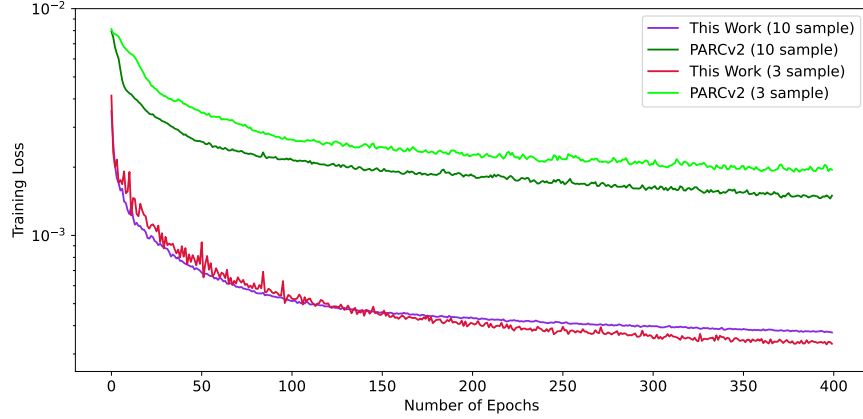


Figure 9: Comparison between the training loss of our model vs. PARCv2 trained on the same meso-scale dataset.

differentiator architecture involves an inductive bias which is motivated by the generalized advection-diffusion-reaction equation.

In order to investigate the performance of both models in the scarce meso-scale data regime, we use a dataset containing 13 instances of shock-initiated reaction simulations in meso-scale microstructures. We consider four training scenarios for each model, using 10, 5, 3 and 1 training samples, respectively. Afterwards, the performance of each model is evaluated on 3 test samples kept separately during the training. Following our two-step meta-learning approach, our model has been trained, initially, on 100 samples of inexpensive micro-scale single-pore collapse simulations. However, PARCv2 is trained from scratch only on the meso-scale data. Figure 9 compares the convergence rate of two models in terms of their training loss in the case of 10 and 3 meso-scale training samples, respectively. We note that pretraining our model on the micro-scale data allows it to start from a lower initial loss value and converge relatively quickly compared to PARCv2, which is trained from scratch using only the meso-scale simulations.

Figure 10 (a) and (b) display the predicted evolution of the temperature field  $T$  by our model and PARCv2, respectively, for a test sample in comparison with the ground-truth numerical simulation. The columns in the figures show the predicted temperature distribution at different instants of time (noted above the panels); the rows correspond to the above-mentioned four scenarios considered for training of each model. The first row shows the ground truth, and the second up to the fifth row illustrate the prediction of each model trained on 10, 5, 3, and 1 meso-scale samples, respectively. In terms of capturing the formation and growth of the hotspots, our model’s prediction outperforms PARCv2, especially in the last three scenarios with few training samples. Our model’s predicted temperature values for the hotspots approaches closer to the ground-truth as the number of training samples increases, but it mostly stays below the ground-truth temperatures. On the other hand, PARCv2 tends to predict fewer hotspots with overpredicted temperature values. The boundary of our model’s predicted hotspots is blurrier compared with PARCv2, *i.e.*, it has less sharp gradients relative to the ambient field. Also, similar observations hold in comparing the predicted evolution of the pressure field  $P$  by our model and PARCv2 as illustrated in Figure 11 (a) and (b), respectively. PARCv2 can better capture the delicate patterns of the shock-waves in the pressure field compared to the present model which can be due to the fact that PARCv2 learns the dynamics in the high-fidelity input space instead of in the VAE-compressed latent space. We extend the comparison between the two models’ performance in terms of quantitative metrics in the following Subsection.

#### 4.4 Quantitative evaluation of prediction performances

In order to further assess the prediction performance of the two models quantitatively, we consider several EM sensitivity metrics which play a crucial role in the design of energetic materials [28]. These quantities of interest (QoI) are defined based on the distribution of the temperature field  $T(x, t)$  over the material domain together with its temporal evolution. Denote by  $\mathbb{D}_{\text{hs}} \subset \mathbb{X}$  the hotspot domain defined as the subregion of the material domain  $\mathbb{X}$  where the temperature of the material exceeds the bulk temperature value  $T_{\text{bulk}}$  after the passage of a planar shock wave, *i.e.*,

$$\mathbb{D}_{\text{hs}} = \{x \in \mathbb{X} \mid T(x) > T_{\text{bulk}}\} . \quad (4.12)$$

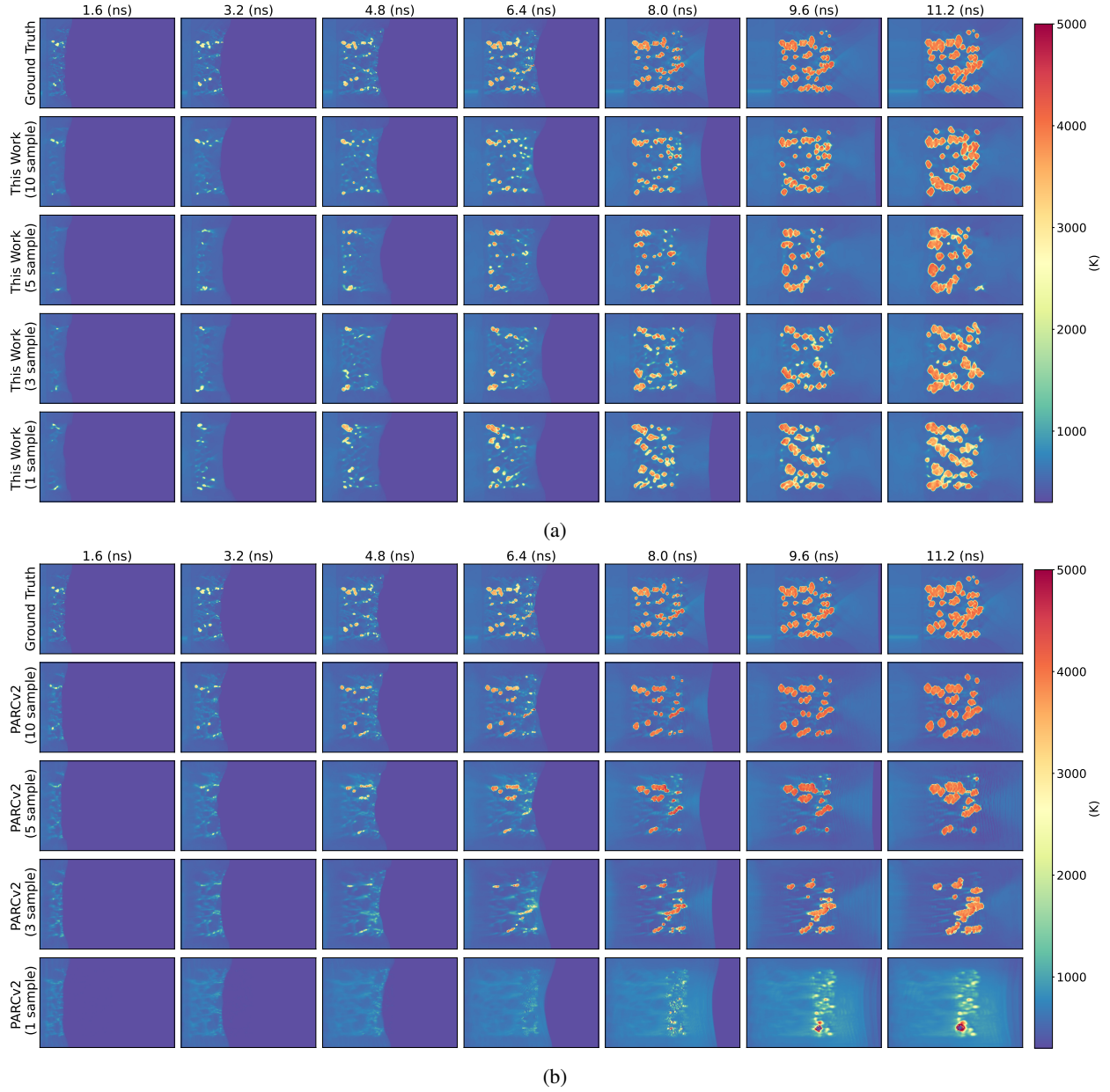


Figure 10: Comparison between the predicted temperature field evolution by (a) our model and (b) PARCv2 in four training scenarios.

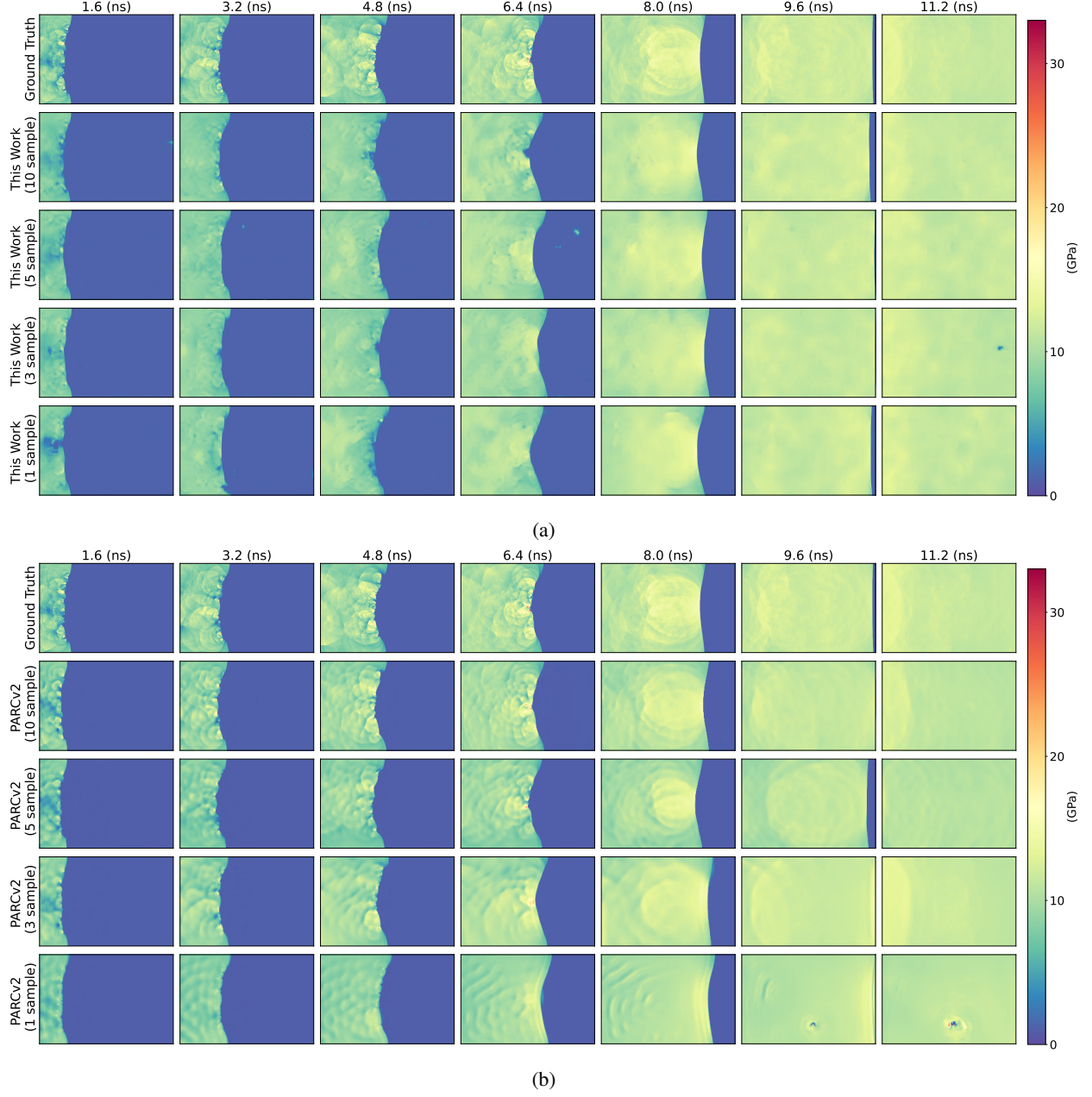


Figure 11: Comparison between the predicted pressure field evolution by (a) our model and (b) PARCv2 in four training scenarios.



Following [29, 17], we consider  $T_{\text{bulk}} = 875$  K in this work. One of the important QoI for determining the sensitivity of an energetic material is the *total hotspot area*  $A_{\text{hs}}$ , which is defined as the area of the hotspot domain  $\mathbb{D}_{\text{hs}}$ , *i.e.*,

$$A_{\text{hs}} = \int_{\mathbb{D}_{\text{hs}}} dx. \quad (4.13)$$

It captures the total contribution of hotspots to shock-induced energy localization in a representative volume element of EMs. The second QoI is the *average hotspot temperature*  $\bar{T}_{\text{hs}}$ , defined by

$$\bar{T}_{\text{hs}} = \frac{1}{A_{\text{hs}}} \int_{\mathbb{D}_{\text{hs}}} T(x) dx, \quad (4.14)$$

which encapsulates the average intensity of localized energy and the likelihood of formation of “critical” hotspots [23]. In addition, the rate of change of the above-mentioned metrics, denoted by  $\dot{A}_{\text{hs}}$  and  $\dot{\bar{T}}_{\text{hs}}$ , respectively, are two other important QoI considered in this work.

Figure 12 (a) and (b) illustrate the time evolution of the total hotspot area  $A_{\text{hs}}$  and the average hotspot temperature  $\bar{T}_{\text{hs}}$  together with their rate of change for our model and PARCv2, respectively, in comparison with the ground-truth (DNS). All of these quantities of interest are calculated based on the predicted evolution of the temperature field for test samples by the two models trained on 10, 5, and 3 meso-scale samples, respectively. In terms of total hotspot area  $A_{\text{hs}}$  and its rate of change  $\dot{A}_{\text{hs}}$ , our model’s prediction shows closer agreement with the ground-truth while PARCv2 tends to underpredict these two QoI. In addition, the overall trend of our model’s predicted average hotspot temperature  $\bar{T}_{\text{hs}}$  is consistent with the ground-truth, although it is underpredicted by  $\sim 350$  K. On the other hand, PARCv2’s prediction of  $\bar{T}_{\text{hs}}$  can be divided into two parts based on the first and the second half of the total time-interval. Roughly speaking, PARCv2 underpredicts  $\bar{T}_{\text{hs}}$  for time-period  $t \in [0, 7.5 \text{ ns}]$  while overpredicts  $\bar{T}_{\text{hs}}$  for  $t \in [7.5 \text{ ns}, 15 \text{ ns}]$ . The sharp increase in PARCv2 predicted  $\bar{T}_{\text{hs}}$  around  $t = 7.5 \text{ ns}$  leads to considerable deviation of its predicted  $\dot{\bar{T}}_{\text{hs}}$  from ground-truth in that region. Figure 13 shows the root mean squared error (RMSE) of the predicted quantities of interest by the two models trained in the aforementioned four scenarios. The RMSE of our model’s predicted total hotspot area  $A_{\text{hs}}$  and its rate of change  $\dot{A}_{\text{hs}}$  is less than %50 of the corresponding RMSE values for PARCv2 in all the training scenarios. On the other hand, the RMSE of PARCv2 predicted average hotspot temperature  $\bar{T}_{\text{hs}}$  decreases much faster than our model by increasing the number of training samples, leading to lower RMSE at the 10-sample training scenario.

#### 4.5 Uncertainty quantification for model prediction

There are two main sources of uncertainty in the predictions made by our model: *i)* the stochasticity due to various morphologies of the input microstructures; *ii)* the stochastic nature of the learned dynamics by our model over the latent space. A comprehensive investigation of these two sources of stochasticity and their relation to each other is an important subject that is beyond the scope of this paper, and we leave it for future work. In this subsection, we focus on the second source of stochasticity as mentioned above, *i.e.*, the uncertainty due to the random sampling made by the variational decoders in our model for predicting the physical fields of interest. We consider the following setup in order to evaluate the uncertainty in our model’s predicted temperature field and sensitivity QoI for the problem of shock-induced energy localization in energetic material. Given the fixed initial condition for all the test samples, we run the model’s inference for 50 trials based on the full *stochastic* dynamics over the latent space, *i.e.*, the evolution of the latent mean field  $\bar{Z}$  and the latent log-variance field  $Z^\sigma$ . We compute the pixel-wise mean and standard deviation of the resulting ensemble of the predicted temperature field  $T$  evolution. In addition, for each test sample, we run the model’s inference based on the *deterministic* dynamics over the corresponding slow manifold, *i.e.*, only the evolution of the latent mean field  $\bar{Z}$ .

Figure 14 illustrates the predicted temperature field  $T$  evolution corresponding to the stochastic and deterministic inference of our model in comparison with the ground-truth for a test sample. The second row shows an instance of stochastic dynamics-based prediction, *i.e.*, a sample from the 50-trial ensemble. The third and fifth rows show the pixel-wise mean-value and standard deviation of the corresponding 50-trial ensemble, respectively. The fourth row illustrates the predicted temperature evolution based on the deterministic dynamics over the latent space. As expected, the mean-value of stochastic dynamics-based predictions is quite close to the deterministic dynamics-based prediction. The standard deviation of predicted  $T$  in the growth stage of hotspots is  $\sim 50$  K. However, in the ignition stage, we see standard deviation up to  $\sim 150$  K, which happens in false positively-predicted ignitions. Figure 15 shows the mean-value and standard deviation of the predicted sensitivity QoI associated with the stochastic dynamics-based 50-trial ensemble, which has been averaged over all the test samples.

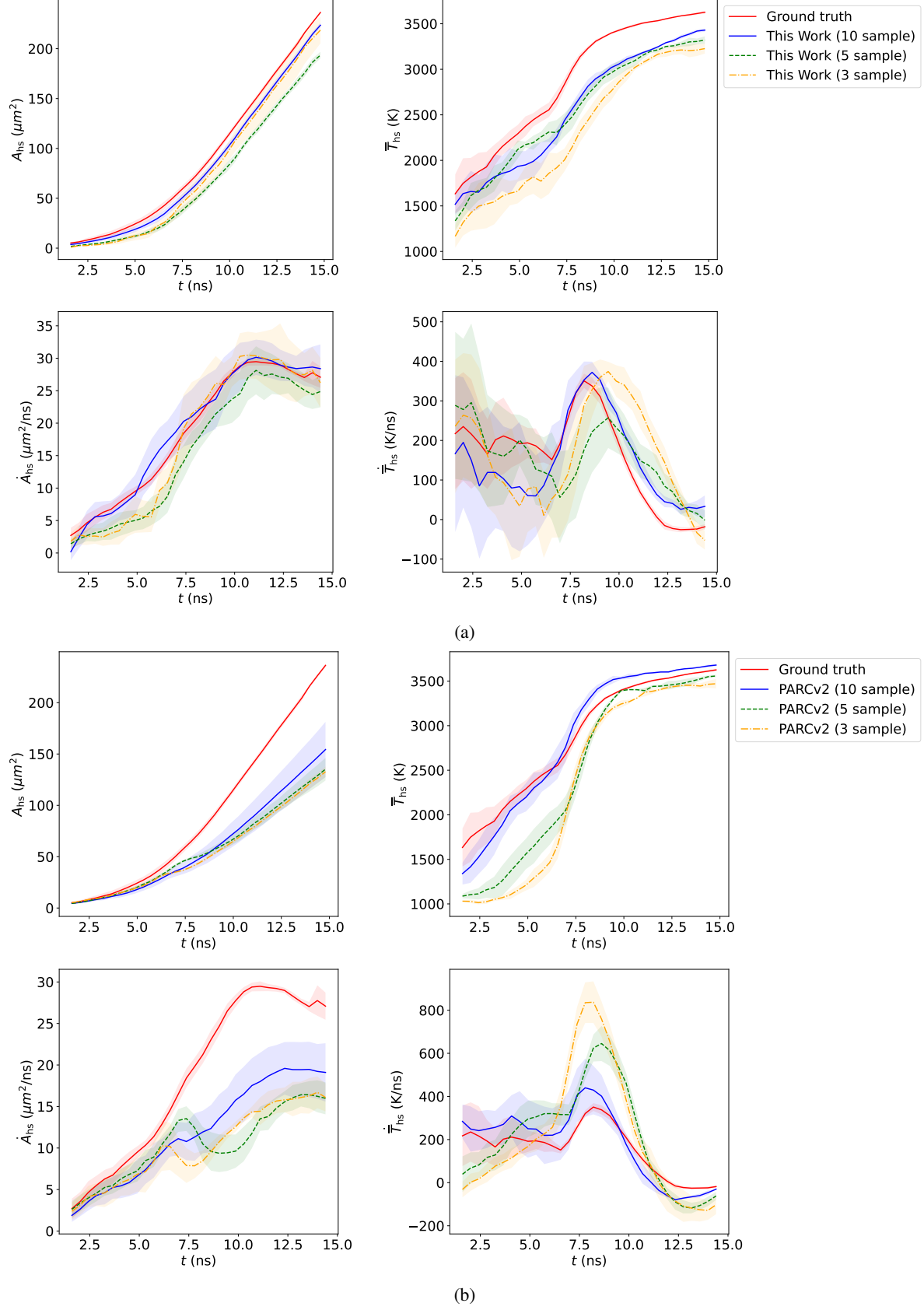


Figure 12: EM sensitivity QoI calculated from (a) our model and (b) PARCv2 prediction in comparison with ground-truth.



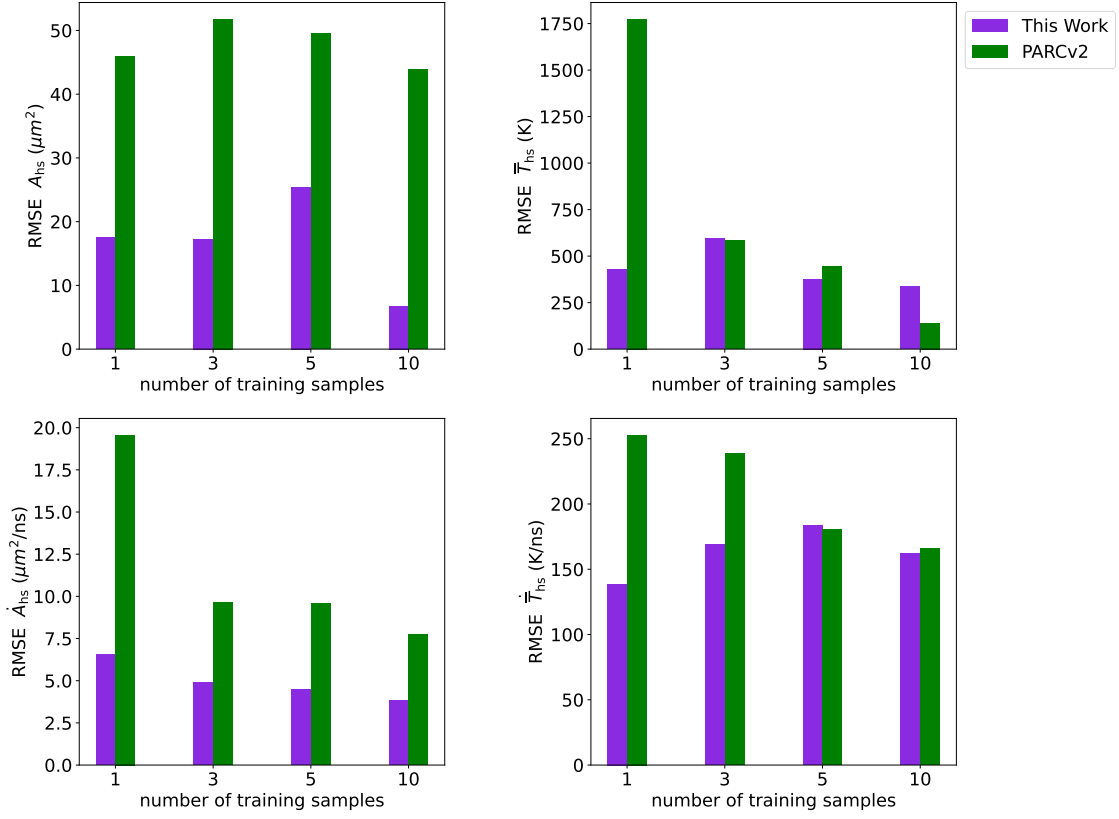


Figure 13: RMSE of the predicted sensitivity QoI by our model and PARCv2 in four training scenarios.

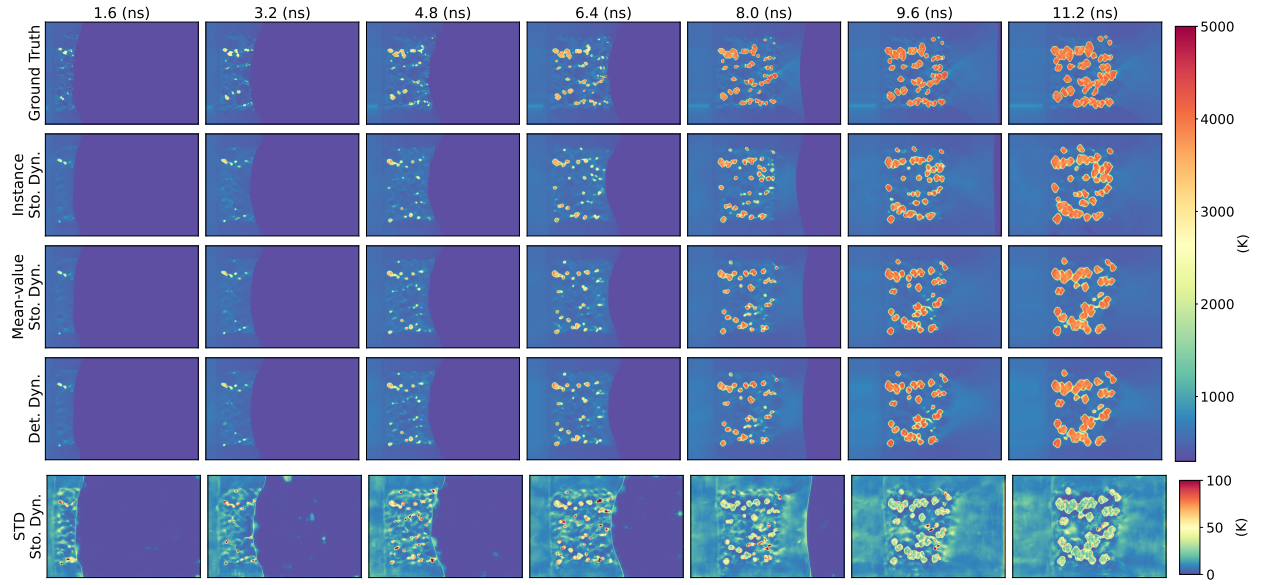


Figure 14: Predicted temperature field evolution based on the stochastic and deterministic dynamics over the latent space.

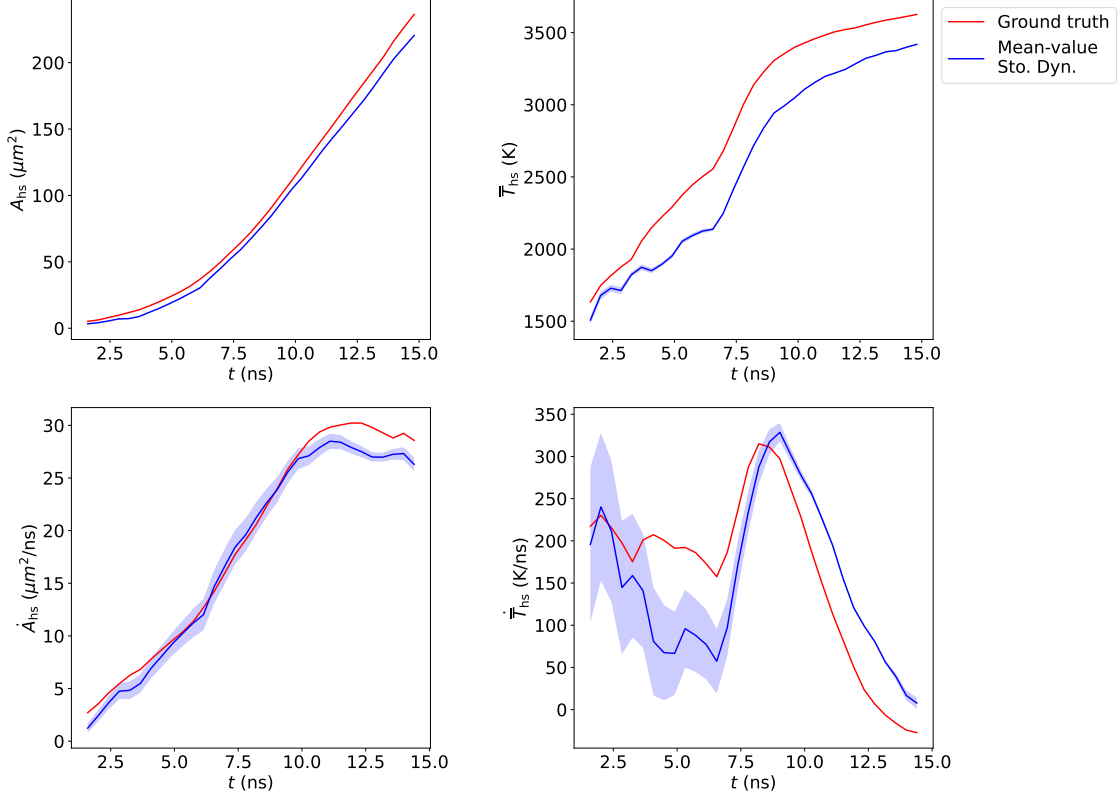


Figure 15: Mean-value and standard deviation of the predicted sensitivity QoI.

## 5 Discussion

This work presented a meta-learning framework for learning the meso-scale thermomechanical behavior of shock-loaded porous energetic material (EM) in a scarce meso-scale data regime by leveraging inexpensive micro-scale simulations. In this framework, it was proposed to consider the corresponding meso-scale dynamics as a composition of interacting building blocks whose dynamics can be learned from micro-scale physics. A probabilistic autoregressive model was suggested to learn a reduced representation of the micro-scale dynamics by capturing the slow manifold associated with the evolution of the temperature and pressure fields in shock-induced single pore collapse in EM. The proposed structure for the autoregressive functional of our model encapsulates the short-term decoupled evolution of the involved physical fields together with their correlated long-term evolution. It was shown that, after learning a latent representation of the micro-scale dynamics, our model can be trained, relatively quickly, on a small dataset of meso-scale simulations in order to learn the higher-order spatiotemporal interactions between the physical fields at meso-scale. Because of the fully convolutional, *i.e.*, CNN-based, architecture of the autoregressive functional, our model is able to learn the correlation between the neighboring micro-scale building blocks of the meso-scale physics.

The predictive capability of our model was compared with a physics-aware recurrent convolutional neural network (PARC) trained only on the same small meso-scale dataset. The results showed that our model could outperform PARC in terms of predicting the formation and advection of localized high temperature regions (hotspots), in addition to the predicted temperature values for the hotspots. Also, the prediction of our model and PARC was compared against the ground-truth numerical simulations in terms of several EM sensitivity metrics which include total hotspot area, average hotspot temperature, and their rate of change over time. The comparison between the prediction performance of our model and PARC trained on the same meso-scale dataset showed that micro-scale dynamics contains crucial information that can considerably help a deep learning-based model to learn the meso-scale physics underlying EM thermo-mechanics.

For future work, we plan to investigate the possibility of performance improvement of our proposed model by considering other neural network architectures, other than the U-Net architecture considered in this work, for the decoupled and the correlation autoregressive functionals. In particular, we expect that the performance of the model can be improved by considering an architecture with hidden states, *e.g.*, Convolutional LSTM [88], which can enhance the

ability of the model in learning the long-term temporal correlations. Additionally, the trade-off between the amount of micro- and meso-scale data which is necessary for training our model needs to be investigated and optimized towards the least possible computational cost in overall. Finally, although the scope of the present work was limited to the thermomechanical behavior of energetic materials, the applicability of the proposed framework to other multiphysics problems with multiscale spatiotemporal dynamics can be a direction of future research.

## Acknowledgments

This work was supported by the National Science Foundation under Grant No. DMREF-2203580.

## Author Declarations

The authors declare that they have no known competing financial interests or personal relationships that could have appeared to influence the work reported in this paper.

## A Appendix

### A.1 Details on Implementation and Training

The encoder of the variational autoencoder in our model has a VGG-Net [75] architecture with no fully-connected layers. It consist of four convolutional blocks with filter size 3, stride 1, rectified linear unit (ReLU) activation function, and number of channels equal to [64, 128, 256, 512], respectively. The output of each convolutional block is down-sampled by a  $2 \times 2$  max-pooling operation with stride 2 to reduce the spatial dimensions by half and, hence, double the size of receptive field. The final feature map with 512 channels is processed through two subsequent convolutional layers with filter size 3, stride 1, no activation function, and number of channels equal to 4, which result in the associated latent-mean and latent-log-variance fields. The decoder has a symmetric architecture to the encoder with the exception that the max-pooling operation is replaced with  $2 \times 2$  up-sampling operation.

All the autoregressive functionals in our model have a U-Net [76] architecture. It consist of a contracting path and an expansive path. The contractive path consist of three convolutional blocks with filter size 3, stride 1, ReLU activation function, and number of channels equal to [64, 128, 256], respectively, where each convolutional block is followed by a  $2 \times 2$  max-pooling operation of stride 2 for down-sampling. The expansive path consist of three convolutional blocks symmetric to the contractive path where the max-pooling operation is replaced with  $2 \times 2$  up-sampling operation followed by a concatenation with corresponding high-resolution feature map from the contractive path.

Our model is trained using the ADAM optimizer [89]. The variational autoencoder corresponding to each physical field is trained for 500 epochs with learning rate  $10^{-5}$ . The autoregressive latent evolution module is trained following a *curriculum learning* [90] strategy in which the predicted time horizon increases successively from 1 to 4. Our model is trained for [400, 300, 300, 200] epochs with learning rates [ $10^{-4}$ ,  $8 \times 10^{-5}$ ,  $6 \times 10^{-5}$ ,  $4 \times 10^{-5}$ ] according to the above-mentioned four-step curriculum learning.

In our experiments, we maintained the same architecture of PARCv2 as presented in [87]. We trained the PARCv2 differentiator with ADAM optimizer following the same curriculum learning setup which was considered for training of the latent evolution module in our model. We did not consider a data-driven integrator for PARCv2 in this experiment and only used the numerical integrator RK4.

### A.2 Numerical Simulation Data

The micro- and meso-scale simulations of the shock-induced energy localization in energetic material considered in this paper are generated using an in-house multi-material flow solver SCIMITAR3D [27, 79, 91]. Details of its numerical framework for computing the reactive shock dynamics in energetic materials are discussed extensively in several publications [26, 92, 93]. Also, its has been validated against experiment [94] and molecular dynamics simulations [95] for high-speed multi-material shock and impact problems.

We use a dataset containing 119 instances of single-pore collapse in addition to 13 instances of meso-scale simulations of shock-initiated reaction in pressed energetic material (Class V HMX [96]). For each simulation instance, the microstructural sample is loaded with a shock applied at the left boundary of the domain with the pressure loading of 9.5 GPa. The shock then traverses through the microstructure from the left to right. The single-pore collapse (*i.e.*, micro-scale) instances have the spatial dimension of  $1.5 \times 2.25(\mu m^2)$  with void diameters ranging from  $0.15(\mu m)$  to

1.5( $\mu m$ ). To capture the intricate details of void collapse and hotspot shapes, the micro-scale simulations employed a range of grid sizes from 0.7( $nm$ ) to 5( $nm$ ). This resulted in computational meshes with approximately  $600 \times 1200$  grid points. The choice of grid size was informed by previous mesh convergence studies on void collapse [79] which indicated that each void should be covered by a minimum of around 200 grid cells to ensure accurate representation (see [31] for details). The calculated temperature  $T$ , pressure  $P$  and microstructural morphology  $\mu$  fields in the micro-scale simulations were recorded at equal time intervals resulting in 19 equally-spaced snapshots with  $\Delta t = 0.17(ns)$ .<sup>8</sup> For training the micro-scale dynamics model, the  $(T, P, \mu)$  snapshots corresponding to the single-pore collapse are resolved with a uniform grid of size  $160 \times 256$  pixels.

The meso-scale microstructure samples have the spatial dimension of  $25 \times 25(\mu m^2)$  padded into a homogeneous HMX material domain of size  $35 \times 51(\mu m^2)$ . In order to capture the same level of physical detail at meso-scale simulations, one needs to use similar grid sizes to the single-pore collapse simulations. However, this leads to computational meshes that are hundreds of times larger than those used in micro-scale simulations. Consequently, this places a significant burden on computational resources, including increased memory usage, longer processing times, and higher computational power requirements (see [29] for details). The calculated evolution of  $(T, P, \mu)$  fields in the meso-scale simulations were recorded at equal time intervals resulting in 38 equally-spaced snapshots with  $\Delta t = 0.4(ns)$  and resolved with a uniform grid of size  $320 \times 480$  pixels.

## References

- [1] Richard Saurel and Rémi Abgrall. A multiphase godunov method for compressible multifluid and multiphase flows. *Journal of Computational Physics*, 150(2):425–467, 1999.
- [2] Holavanahalli S Udaykumar, Heng-Chuan Kan, Wei Shyy, and Roger Tran-Son-Tay. Multiphase dynamics in arbitrary geometries on fixed cartesian grids. *Journal of Computational Physics*, 137(2):366–405, 1997.
- [3] Laura M McDowell-Boyer, James R Hunt, and Nicholas Sitar. Particle transport through porous media. *Water resources research*, 22(13):1901–1921, 1986.
- [4] JC Parker. Multiphase flow and transport in porous media. *Reviews of Geophysics*, 27(3):311–328, 1989.
- [5] Hong Luo, Joseph D Baum, and Rainald Löhner. On the computation of multi-material flows using ale formulation. *Journal of Computational Physics*, 194(1):304–328, 2004.
- [6] Jeffrey W Banks, Donald W Schwendeman, Ashwana K Kapila, and William D Henshaw. A high-resolution godunov method for compressible multi-material flow on overlapping grids. *Journal of Computational Physics*, 223(1):262–297, 2007.
- [7] W Lee Perry, Brad Clements, Xia Ma, and Joseph T Mang. Relating microstructure, temperature, and chemistry to explosive ignition and shock sensitivity. *Combustion and flame*, 190:171–176, 2018.
- [8] Jacob Fish. *Multiscale methods: bridging the scales in science and engineering*. Oxford University Press, 2010.
- [9] Wing Kam Liu, Harold S Park, Dong Qian, Eduard G Karpov, Hiroshi Kadowaki, and Gregory J Wagner. Bridging scale methods for nanomechanics and materials. *Computer Methods in Applied Mechanics and Engineering*, 195(13-16):1407–1421, 2006.
- [10] Richard Saurel, François Fraysse, Damien Furfaro, and Emmanuel Lapebie. Multiscale multiphase modeling of detonations in condensed energetic materials. *Computers & Fluids*, 169:213–229, 2018.
- [11] Benjamin Sanderse, Panos Stinis, Romit Maulik, and Shady E Ahmed. Scientific machine learning for closure models in multiscale problems: A review. *arXiv preprint arXiv:2403.02913*, 2024.
- [12] Andrea Beck, David Flad, and Claus-Dieter Munz. Deep neural networks for data-driven les closure models. *Journal of Computational Physics*, 398:108910, 2019.
- [13] Omer San and Romit Maulik. Neural network closures for nonlinear model order reduction. *Advances in Computational Mathematics*, 44(6):1717–1750, 2018.
- [14] Yann LeCun, Yoshua Bengio, and Geoffrey Hinton. Deep learning. *nature*, 521(7553):436–444, 2015.
- [15] Yoshua Bengio, Ian Goodfellow, and Aaron Courville. *Deep learning*, volume 1. MIT press Cambridge, MA, USA, 2017.
- [16] George Em Karniadakis, Ioannis G Kevrekidis, Lu Lu, Paris Perdikaris, Sifan Wang, and Liu Yang. Physics-informed machine learning. *Nature Reviews Physics*, 3(6):422–440, 2021.

<sup>8</sup>In the numerical simulation, in order to capture the sharp interface between voids and the HMX substrate, the interfaces are modeled using the narrow band levelset approach [97, 31]. However, the microstructural morphology field  $\mu$ , considered in this paper for training the neural network models, is a binarized version of the levelset representation.

- [17] Phong CH Nguyen, Yen-Thi Nguyen, Joseph B Choi, Pradeep K Seshadri, HS Udaykumar, and Stephen S Baek. Parc: Physics-aware recurrent convolutional neural networks to assimilate meso scale reactive mechanics of energetic materials. *Science advances*, 9(17):eadd6868, 2023.
- [18] Karthik Kashinath, M Mustafa, Adrian Albert, JL Wu, C Jiang, Soheil Esmaeilzadeh, Kamyar Azizzadenesheli, R Wang, Ashesh Chattopadhyay, A Singh, et al. Physics-informed machine learning: case studies for weather and climate modelling. *Philosophical Transactions of the Royal Society A*, 379(2194):20200093, 2021.
- [19] Vivek Oommen, Khemraj Shukla, Saaketh Desai, Rémi Dingreville, and George Em Karniadakis. Rethinking materials simulations: Blending direct numerical simulations with neural operators. *npj Computational Materials*, 10(1):145, 2024.
- [20] MR Baer. Modeling heterogeneous energetic materials at the mesoscale. *Thermochimica acta*, 384(1-2):351–367, 2002.
- [21] John E Field. Hot spot ignition mechanisms for explosives. *Accounts of chemical Research*, 25(11):489–496, 1992.
- [22] Ralph Menikoff. Pore collapse and hot spots in hmx. In *AIP Conference Proceedings*, volume 706, pages 393–396. American Institute of Physics, 2004.
- [23] Craig M Tarver, Steven K Chidester, and Albert L Nichols. Critical conditions for impact-and shock-induced hot spots in solid explosives. *The Journal of Physical Chemistry*, 100(14):5794–5799, 1996.
- [24] CA Handley, BD Lambourn, NJ Whitworth, HR James, and WJ Belfield. Understanding the shock and detonation response of high explosives at the continuum and meso scales. *Applied Physics Reviews*, 5(1), 2018.
- [25] Richard R Bernecker. The deflagration-to-detonation transition process for high-energy propellants-a review. *AIAA journal*, 24(1):82–91, 1986.
- [26] A Kapahi and HS Udaykumar. Dynamics of void collapse in shocked energetic materials: physics of void–void interactions. *Shock Waves*, 23:537–558, 2013.
- [27] Nirmal K Rai and HS Udaykumar. Mesoscale simulation of reactive pressed energetic materials under shock loading. *Journal of Applied Physics*, 118(24), 2015.
- [28] O Sen, NK Rai, AS Diggs, DB Hardin, and HS Udaykumar. Multi-scale shock-to-detonation simulation of pressed energetic material: A meso-informed ignition and growth model. *Journal of Applied Physics*, 124(8), 2018.
- [29] Pradeep K Seshadri, Yen T Nguyen, Oishik Sen, and HS Udaykumar. Meso-scale simulation of energetic materials. ii. establishing structure–property linkages using synthetic microstructures. *Journal of Applied Physics*, 131(5), 2022.
- [30] Yen T. Nguyen, Pradeep K. Seshadri, Oishik Sen, David B. Hardin, Christopher D. Molek, and H. S. Udaykumar. Multi-scale modeling of shock initiation of a pressed energetic material. ii. effect of void–void interactions on energy localization. *Journal of Applied Physics*, 131(21):215903, 2022.
- [31] Yen Nguyen, Pradeep Seshadri, Oishik Sen, D Barrett Hardin, Christopher D Molek, and HS Udaykumar. Multi-scale modeling of shock initiation of a pressed energetic material i: The effect of void shapes on energy localization. *Journal of Applied Physics*, 131(5), 2022.
- [32] Timothy Hospedales, Antreas Antoniou, Paul Micaelli, and Amos Storkey. Meta-learning in neural networks: A survey. *IEEE transactions on pattern analysis and machine intelligence*, 44(9):5149–5169, 2021.
- [33] Hung-yi Lee, Shang-Wen Li, and Ngoc Thang Vu. Meta learning for natural language processing: A survey. *arXiv preprint arXiv:2205.01500*, 2022.
- [34] Sinno Jialin Pan and Qiang Yang. A survey on transfer learning. *IEEE Transactions on knowledge and data engineering*, 22(10):1345–1359, 2009.
- [35] Emilio Soria Olivas, Jos David Mart Guerrero, Marcelino Martinez-Sober, Jose Rafael Magdalena-Benedito, L Serrano, et al. *Handbook of research on machine learning applications and trends: Algorithms, methods, and techniques: Algorithms, methods, and techniques*. IGI global, 2009.
- [36] Alfio Quarteroni, Gianluigi Rozza, et al. *Reduced order methods for modeling and computational reduction*, volume 9. Springer, 2014.
- [37] Gal Berkooz, Philip Holmes, and John L Lumley. The proper orthogonal decomposition in the analysis of turbulent flows. *Annual review of fluid mechanics*, 25(1):539–575, 1993.
- [38] Peter J Schmid. Dynamic mode decomposition of numerical and experimental data. *Journal of fluid mechanics*, 656:5–28, 2010.

- [39] Kookjin Lee and Kevin T Carlberg. Model reduction of dynamical systems on nonlinear manifolds using deep convolutional autoencoders. *Journal of Computational Physics*, 404:108973, 2020.
- [40] Aleksandr Nikolaevich Gorban and Ilya V Karlin. *Invariant manifolds for physical and chemical kinetics*, volume 660. Springer, 2005.
- [41] Jack Carr. *Applications of centre manifold theory*, volume 35. Springer Science & Business Media, 2012.
- [42] Peter Benner, Serkan Gugercin, and Karen Willcox. A survey of projection-based model reduction methods for parametric dynamical systems. *SIAM review*, 57(4):483–531, 2015.
- [43] Stefania Fresca, Luca Dede’, and Andrea Manzoni. A comprehensive deep learning-based approach to reduced order modeling of nonlinear time-dependent parametrized pdes. *Journal of Scientific Computing*, 87:1–36, 2021.
- [44] Rudy Geelen, Stephen Wright, and Karen Willcox. Operator inference for non-intrusive model reduction with quadratic manifolds. *Computer Methods in Applied Mechanics and Engineering*, 403:115717, 2023.
- [45] Romit Maulik, Bethany Lusch, and Prasanna Balaprakash. Reduced-order modeling of advection-dominated systems with recurrent neural networks and convolutional autoencoders. *Physics of Fluids*, 33(3), 2021.
- [46] Youngkyu Kim, Youngsoo Choi, David Widemann, and Tarek Zohdi. A fast and accurate physics-informed neural network reduced order model with shallow masked autoencoder. *Journal of Computational Physics*, 451:110841, 2022.
- [47] William D Fries, Xiaolong He, and Youngsoo Choi. Lasdi: Parametric latent space dynamics identification. *Computer Methods in Applied Mechanics and Engineering*, 399:115436, 2022.
- [48] Pantelis R Vlachas, Georgios Arampatzis, Caroline Uhler, and Petros Koumoutsakos. Multiscale simulations of complex systems by learning their effective dynamics. *Nature Machine Intelligence*, 4(4):359–366, 2022.
- [49] Paolo Conti, Giorgio Gobat, Stefania Fresca, Andrea Manzoni, and Attilio Frangi. Reduced order modeling of parametrized systems through autoencoders and sindy approach: continuation of periodic solutions. *Computer Methods in Applied Mechanics and Engineering*, 411:116072, 2023.
- [50] Christophe Bonneville, Youngsoo Choi, Debojyoti Ghosh, and Jonathan L Belof. Gplasdi: Gaussian process-based interpretable latent space dynamics identification through deep autoencoder. *Computer Methods in Applied Mechanics and Engineering*, 418:116535, 2024.
- [51] Diederik P Kingma and Max Welling. Auto-encoding variational bayes. *Proceedings of the 2nd International Conference on Learning representations (ICLR)*, 2014.
- [52] Jürgen Schmidhuber. *Evolutionary principles in self-referential learning, or on learning how to learn: the meta-meta-... hook*. PhD thesis, Technische Universität München, 1987.
- [53] Yoshua Bengio, Samy Bengio, and Jocelyn Cloutier. *Learning a synaptic learning rule*. Citeseer, 1990.
- [54] Sebastian Thrun and Lorien Pratt. *Learning to learn*. Springer Science & Business Media, 1998.
- [55] Michael Penwarden, Shandian Zhe, Akil Narayan, and Robert M Kirby. A metalearning approach for physics-informed neural networks (pinns): Application to parameterized pdes. *Journal of Computational Physics*, 477:111912, 2023.
- [56] Marcin Andrychowicz, Misha Denil, Sergio Gomez, Matthew W Hoffman, David Pfau, Tom Schaul, Brendan Shillingford, and Nando De Freitas. Learning to learn by gradient descent by gradient descent. *Advances in neural information processing systems*, 29, 2016.
- [57] Sachin Ravi and Hugo Larochelle. Optimization as a model for few-shot learning. In *International conference on learning representations*, 2017.
- [58] Luca Franceschi, Paolo Frasconi, Saverio Salzo, Riccardo Grazi, and Massimiliano Pontil. Bilevel programming for hyperparameter optimization and meta-learning. In *International conference on machine learning*, pages 1568–1577. PMLR, 2018.
- [59] Gregory Koch, Richard Zemel, Ruslan Salakhutdinov, et al. Siamese neural networks for one-shot image recognition. In *ICML deep learning workshop*, volume 2, pages 1–30. Lille, 2015.
- [60] Oriol Vinyals, Charles Blundell, Timothy Lillicrap, Daan Wierstra, et al. Matching networks for one shot learning. *Advances in neural information processing systems*, 29, 2016.
- [61] Jake Snell, Kevin Swersky, and Richard Zemel. Prototypical networks for few-shot learning. *Advances in neural information processing systems*, 30, 2017.
- [62] Sepp Hochreiter, A Steven Younger, and Peter R Conwell. Learning to learn using gradient descent. In *Artificial Neural Networks—ICANN 2001: International Conference Vienna, Austria, August 21–25, 2001 Proceedings 11*, pages 87–94. Springer, 2001.

- [63] Adam Santoro, Sergey Bartunov, Matthew Botvinick, Daan Wierstra, and Timothy Lillicrap. Meta-learning with memory-augmented neural networks. In *International conference on machine learning*, pages 1842–1850. PMLR, 2016.
- [64] Nikhil Mishra, Mostafa Rohaninejad, Xi Chen, and Pieter Abbeel. A simple neural attentive meta-learner. *arXiv preprint arXiv:1707.03141*, 2017.
- [65] Maziar Raissi, Paris Perdikaris, and George E Karniadakis. Physics-informed neural networks: A deep learning framework for solving forward and inverse problems involving nonlinear partial differential equations. *Journal of Computational physics*, 378:686–707, 2019.
- [66] Xu Liu, Xiaoya Zhang, Wei Peng, Weien Zhou, and Wen Yao. A novel meta-learning initialization method for physics-informed neural networks. *Neural Computing and Applications*, 34(17):14511–14534, 2022.
- [67] Apostolos F Psaros, Kenji Kawaguchi, and George Em Karniadakis. Meta-learning pinn loss functions. *Journal of computational physics*, 458:111121, 2022.
- [68] Alex Bihlo. Improving physics-informed neural networks with meta-learned optimization. *Journal of Machine Learning Research*, 25(14):1–26, 2024.
- [69] Roger Temam. *Infinite-dimensional dynamical systems in mechanics and physics*, volume 68. Springer Science & Business Media, 2012.
- [70] Philip Holmes, John L Lumley, Gahl Berkooz, and Clarence W Rowley. *Turbulence, coherent structures, dynamical systems and symmetry*. Cambridge university press, 2012.
- [71] Danilo Jimenez Rezende, Shakir Mohamed, and Daan Wierstra. Stochastic backpropagation and approximate inference in deep generative models. In *International conference on machine learning*, pages 1278–1286. PMLR, 2014.
- [72] Havard Rue and Leonhard Held. *Gaussian Markov random fields: theory and applications*. Chapman and Hall/CRC, 2005.
- [73] Jürgen Schmidhuber. Deep learning in neural networks: An overview. *Neural networks*, 61:85–117, 2015.
- [74] Stéphane Mallat. Understanding deep convolutional networks. *Philosophical Transactions of the Royal Society A: Mathematical, Physical and Engineering Sciences*, 374(2065):20150203, 2016.
- [75] Karen Simonyan. Very deep convolutional networks for large-scale image recognition. *arXiv preprint arXiv:1409.1556*, 2014.
- [76] Olaf Ronneberger, Philipp Fischer, and Thomas Brox. U-net: Convolutional networks for biomedical image segmentation. In *Medical image computing and computer-assisted intervention–MICCAI 2015: 18th international conference, Munich, Germany, October 5-9, 2015, proceedings, part III 18*, pages 234–241. Springer, 2015.
- [77] Tailin Wu, Takashi Maruyama, and Jure Leskovec. Learning to accelerate partial differential equations via latent global evolution. *Advances in Neural Information Processing Systems*, 35:2240–2253, 2022.
- [78] S Sambasivan, Anil Kapahi, and HS Udaykumar. Simulation of high speed impact, penetration and fragmentation problems on locally refined cartesian grids. *Journal of Computational Physics*, 235:334–370, 2013.
- [79] Nirmal Kumar Rai, Martin J Schmidt, and HS Udaykumar. High-resolution simulations of cylindrical void collapse in energetic materials: Effect of primary and secondary collapse on initiation thresholds. *Physical Review Fluids*, 2(4):043202, 2017.
- [80] HS Udaykumar, Oishik Sen, Sangyup Lee, and Nirmal K Rai. Unified approach for meso-informed burn models in shocked energetic materials. *Journal of propulsion and power*, 36(5):655–667, 2020.
- [81] Charles L Mader. *Numerical modeling of explosives and propellants*. CRC press, 2007.
- [82] Kevin R Moon, David Van Dijk, Zheng Wang, Scott Gigante, Daniel B Burkhardt, William S Chen, Kristina Yim, Antonia van den Elzen, Matthew J Hirn, Ronald R Coifman, et al. Visualizing structure and transitions in high-dimensional biological data. *Nature biotechnology*, 37(12):1482–1492, 2019.
- [83] Ronald R Coifman and Stéphane Lafon. Diffusion maps. *Applied and computational harmonic analysis*, 21(1):5–30, 2006.
- [84] Edward L Lee and Craig M Tarver. Phenomenological model of shock initiation in heterogeneous explosives. *The Physics of Fluids*, 23(12):2362–2372, 1980.
- [85] R Menikoff and Milton S Shaw. Reactive burn models and ignition & growth concept. In *EPJ Web of Conferences*, volume 10, page 00003. EDP Sciences, 2010.

- [86] Wenjie Luo, Yujia Li, Raquel Urtasun, and Richard Zemel. Understanding the effective receptive field in deep convolutional neural networks. *Advances in neural information processing systems*, 29, 2016.
- [87] Phong C.H Nguyen, Xinlun Cheng, Shahab Azarfar, Pradeep Seshadri, Yen T. Nguyen, Munho Kim, Sanghun Choi, H. S. Udaykumar, and Stephen Baek. Parcv2: Physics-aware recurrent convolutional neural networks for spatiotemporal dynamics modeling. In *Proceedings of the 41st International Conference on Machine Learning, ICML'24*. JMLR.org, 2025.
- [88] Xingjian Shi, Zhourong Chen, Hao Wang, Dit-Yan Yeung, Wai-Kin Wong, and Wang-chun Woo. Convolutional lstm network: A machine learning approach for precipitation nowcasting. *Advances in neural information processing systems*, 28, 2015.
- [89] Diederik P Kingma and Jimmy Ba. Adam: A method for stochastic optimization. *Proceedings of International Conference on Learning Representations*, 2015.
- [90] Petru Soviany, Radu Tudor Ionescu, Paolo Rota, and Nicu Sebe. Curriculum learning: A survey. *International Journal of Computer Vision*, 130(6):1526–1565, 2022.
- [91] Nirmal Kumar Rai and HS Udaykumar. Three-dimensional simulations of void collapse in energetic materials. *Physical Review Fluids*, 3(3):033201, 2018.
- [92] Nirmal Kumar Rai, Martin J Schmidt, and HS Udaykumar. Collapse of elongated voids in porous energetic materials: Effects of void orientation and aspect ratio on initiation. *Physical Review Fluids*, 2(4):043201, 2017.
- [93] Pratik Das and HS Udaykumar. A sharp-interface method for the simulation of shock-induced vaporization of droplets. *Journal of Computational Physics*, 405:109005, 2020.
- [94] NK Rai, SP Koundinyan, O Sen, IV Schweigert, BF Henson, and HS Udaykumar. Evaluation of reaction kinetics models for meso-scale simulations of hotspot initiation and growth in hmx. *Combustion and Flame*, 219:225–241, 2020.
- [95] Pratik Das, Puhan Zhao, Dilki Perera, Tommy Sewell, and HS Udaykumar. Molecular dynamics-guided material model for the simulation of shock-induced pore collapse in  $\beta$ -octahydro-1, 3, 5, 7-tetranitro-1, 3, 5, 7-tetrazocine ( $\beta$ -hmx). *Journal of Applied Physics*, 130(8), 2021.
- [96] CD Molek, EJ Welle, RR Wixom, MB Ritchey, P Samuels, and Y Horie. Microstructural characterization of pressed hmx material sets at differing densities. In *AIP Conference Proceedings*, volume 1793. AIP Publishing, 2017.
- [97] James Sethian. *Level Set Methods and Fast Marching Methods: Evolving Interfaces in Computational Geometry, Fluid Mechanics, Computer Vision, and Materials Science*. Cambridge University Press, 1996.